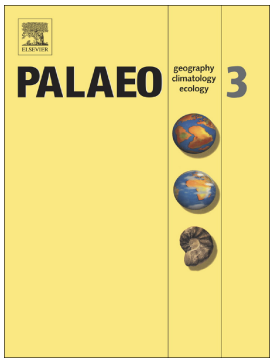

Magnetic susceptibility in the European Loess Belt: New and existing models of magnetic enhancement in loess

Balázs Bradák, Yusuke Seto, Thomas Stevens, Gábor Újvári, Katalin Fehér, Chiara Költringer

PII: S0031-0182(21)00114-0

DOI: https://doi.org/10.1016/j.palaeo.2021.110329

Reference: PALAEO 110329

To appear in: *Palaeogeography, Palaeoclimatology, Palaeoecology*

Received date: 27 October 2020

Revised date: 17 February 2021

Accepted date: 23 February 2021

Please cite this article as: B. Bradák, Y. Seto, T. Stevens, et al., Magnetic susceptibility in the European Loess Belt: New and existing models of magnetic enhancement in loess, *Palaeogeography, Palaeoclimatology, Palaeoecology* (2021), https://doi.org/10.1016/j.palaeo.2021.110329

Magnetic susceptibility in the European Loess Belt: new and existing models of magnetic enhancement in loess

Balázs Bradák[1,*], Yusuke Seto[2], Thomas Stevens[3], Gábor Újvári[4,5], Katalin Fehér[6], Chiara Költringer[3]

[1]Department of Physics, University of Burgos, Av. de Cantabria, s/n 09006, Burgos, Spain

[2]Department of Planetology, Kobe University, Nada, Kobe, 657-8501, Japan

[3]Department of Earth Sciences, Uppsala University, Villavägen 16, Uppsala, 75236, Sweden

[4]Department of Lithospheric Research, Univ. of Vienna, 14 Althanstrasse, Vienna, Austria, A-1090

[5]Institute for Geological and Geochemical Research, Research Centre for Astronomy and Earth Sciences, 45 Budaörsi St., Budapest, Hungary, H-1112.

[6] ELTE Eötvös Loránd University, Institute of Geography and Earth Sciences, Department of Environmental and Landscape Geography, Pázmány Péter sétány 1/C. Budapest, Hungary, H-1117

*Corresponding author: Balázs Bradák, bradak.b@gmail.com

Yusuke Seto: seto@crystal.kobe-u.ac.jp; Thomas Stevens: thomas.stevens@geo.uu.se; Gábor Újvári: Ujvari.Gabor@csfk.mta.hu; Katalin Fehér: feher.katoke@gmail.com; Chiara Költringer: chiara.koltringer@geo.uu.se

Abstract

Magnetic susceptibility measurements play a key role in Quaternary studies. Magnetic proxies, such as low field and frequency-dependent magnetic susceptibility, are widely applied in the reconstruction of terrestrial paleoclimate, e.g., in the study of loess-paleosol successions. In general, the interpretation of loess magnetic susceptibility signals is based on two commonly accepted models: the pedogenic magnetic enhancement and wind-vigour models. However, there are an increasing number of cases where such models cannot be used. These cases show unusual relationships between the two common loess magnetic susceptibility proxies: low field and frequency-dependent magnetic susceptibility. Such relationships have been attributed to various phenomena including the dissolution of fine-grain minerals and the formation of

ultrafine magnetic rims on the surface of coarser grains by weathering. Despite the growing number of these exceptional cases of magnetic enhancement, our knowledge about the occurrence and potential causes of the unusual behaviour of magnetic susceptibility parameters is still limited. This, in turn, hinders the wider application of magnetic susceptibility parameters in loess. To fill this knowledge gap, magnetic susceptibility data of various profiles from the European Loess Belt were collected and compared to reveal various enhancement trends in loess. Along with the analysis of magnetic susceptibility parameters, combined scanning electron microscopy (SEM) and rock magnetic analyses were applied to samples from the Paks loess sequence in Hungary to describe some of the irregular cases, notably the cause of increasing frequency-dependent susceptibility in non-altered sediments. Analysis of loess, paleosol and common mineral samples separated from loess (e.g., muscovite) revealed that various features may be responsible for these increasing frequency-dependent susceptibility values: i) surface weathering (maghemitization) of coarser detrital grains, ii) nanofragmentation by physical weathering and iii) the appearance of significant amounts of ultrafine magnetic inclusions in micas. These special modes of magnetic enhancement of loess do not undermine the importance of the basic theories suggested above, but rather provide three mechanisms that account for some of the increasing

number of unusual cases. To aid in the wider and more accurate use of magnetic susceptibility parameters in loess, we review the current magnetic enhancement models with special emphasis on the identification of unusual trends in magnetic enhancement and understanding their drivers.

Keywords: magnetic susceptibility; loess; magnetic enhancement; nano-scale fragmentation; magnetic inclusion

Abbreviations: CLP-Chinese Loess Plateau; EDS-energy-dispersive X-ray spectroscopy; ELB-European Loess Belt; EXT-extract by strong magnet; χ_{lf}-low field magnetic susceptibility; χ_{fd}-frequency dependent magnetic susceptibility; χ_{fs}-normalized frequency dependent magnetic susceptibility; MIS-marine isotope stage; MD-multidomain; PSD-pseudo-single domain; RESIDc-coarser grained (>125 μm) residual after extraction by strong magnet; RESIDf-finer grained (<125 μm) residual after extraction by strong magnet; SD-single domain; SEM-scanning electron microscope; SP-superparamagnetic; Tc-Curie temperature; VS-vortex state;

1. Introduction

The nature of glacial and interglacial paleoenvironments and their role in understanding future climates has become a major focus of Quaternary research over recent decades (PAGES, 2016). As a part of the reconstruction of paleoenvironment, increasingly more information has been revealed about loess records, which are some of the most commonly used terrestrial archives in the reconstruction of glacial and interglacial paleoenvironment over the Quaternary (Pye, 1987). In such reconstructions, mineral magnetic methods play a crucial role since both the type and amount of magnetic contributors in loess are highly sensitive to environmental change during pedogenesis (Maher and Taylor, 1988; Heller et al., 1993; Forster et al., 1994; Dearing et al., 1996; Maher, 2011, 2016). In fact, basic frequency-dependent magnetic susceptibility analysis has become a routine stratigraphic tool in studies of loess sequences (e.g., Schatzel et al. 2018 and references therein).

There are two commonly known models for the enhancement of the magnetic susceptibility parameters in loess: pedogenesis and wind vigour (e.g., Forster et al., 1994; Evans and Heller, 1994; Evans, 2001). Both models were built to describe the rhythmic change of environmental magnetic proxies, especially magnetic susceptibility

parameters, in loess sequences, most likely related to the cycles of glacial (stadial) and interglacial (interstadial) periods. The widely accepted main magnetic enhancement models seem highly variable geographically. Additionally, there is no consensus about the applicability of the alternative models, and apparently, a number of different hypotheses appear in the literature (see Section 2). Due to the common use of χ_{lf} and χ_{fd}, it is essential to resolve these inconsistencies and ambiguities so that these widely used proxies can properly inform debates about past environmental changes. This requires understanding of the fundamental physical meaning of magnetic parameters. The primary goal of this study is to reveal potential influences on magnetic mineral components in sediments that exhibit unusual χ_{lf} and χ_{fd} using examples from the Paks loess section in Hungary.

2. The overview of magnetic enhancement models in loess characterized by the relationship between χ_{lf} and χ_{fd} parameters

2.1 Pedogenic enhancement model and the "true loess line"

The pedogenic model explains the magnetic enhancement of loess by in situ

authigenic mineral formation (Maher and Taylor, 1988; Heller et al., 1993; Forster et al., 1994; Dearing et al., 1996; Maher, 2011, 2016). This leads to increased low field magnetic susceptibilities (χ_{lf}) and frequency-dependent magnetic susceptibilities (χ_{fd}) in soils formed over interglacials, offering favourable conditions for the formation of ultrafine superparamagnetic (SP) components, such as warmer temperatures and more humid environments (higher precipitation). This relationship between precipitation and mineral neoformation allows for quantitative paleoprecipitation estimation using mineral magnetic methods (e.g., Heller et al., 1993; Maher et al., 1994, 2002, 2003; Panaiotu et al., 2001; Geiss and Zanner, 2007; Geiss et al., 2008; Balsam et al., 2011; Orgeira et al., 2011; Long et al., 2016).

One of the commonly applied mineral magnetic methods used in paleoprecipitation estimation is the measurement of χ_{fd}. χ_{fd} analysis has been applied since the pioneering studies of Forster et al. (1994) and Dearing et al. (1996) as a sensitive indicator of ultrafine magnetic grains, increasing amounts of which also influence χ_{lf}. This linear relationship between increasing χ_{fd} and χ_{lf} was recognized in many loess successions of the European Loess Belt (ELB) and the Chinese Loess Plateau (CLP) and is called the pedogenic enhancement model (Zhou et al., 1990; Forster et al., 1994; Evans and Heller, 1994; Evans, 2001). The relationship between the two susceptibility parameters, i.e., the

trend described by χ_{lf} and χ_{fd}, has been used since publication of the above studies to recognize pedogenic enhancement in loess sequences (e.g., Maher, 2011; Maher, 2016, and the references therein). Following the study of Maher (2016), where the magnetic enhancement models were summarized, Zeeden et al. (2016, 2018) defined the so-called true loess line. The "true loess line" is a linear trend fitted to χ_{lf} and χ_{fd} data, describing the magnetic enhancement trend of loess during pedogenesis driven by increasing neoformation of magnetic minerals. Although the term "true loess line" was first introduced in Zeeden et al. (2016), variations of the χ_{lf} vs. χ_{fd} plot and the "true loess" trend have been commonly used since the loess studies of the 1990s (e.g., Forster et al., 1994; Panaiotu et al., 2001; Maher, 2011).

2.2 Deviation from "true loess line" and other enhancement models

As summarized by Maher (2011) and Zeeden et al. (2018), deviation from the "true loess line" may indicate additional processes that, along with pedogenesis, contribute to the magnetic enhancement of loess. The deviations appear in various ways in the χ_{lf} vs. χ_{fd} plot. Compared with pedogenic enhancement, some loess sequences are characterized by relatively high χ_{lf} compared with the soil horizons (e.g., Begét and Hawkins, 1989). In other cases, some well-developed soil horizons may not show high

χ_{fd} values (e.g., Taylor et al., 2014). There are sediments surprisingly characterized by low χ_{lf} but relatively high χ_{fd} (Wacha et al., 2018). In this sense, the "true loess line" does not seem to be always applicable to loess records, as there are loess deposits in the broader sense of wind-blown terrestrial silt deposits showing deviations from this line. Such discrepancies and their possible causes are described in detail below.

2.2.1 Wind-vigour model

In contrast to the pedogenic model, the wind-vigour model explains observations of higher χ_{lf} values in loess (rather than palaeosols) as a result of the enrichment of coarser grained magnetic minerals in the units of coarse grained loess (Evans, 2001). Increasing magnetic susceptibility during glacial periods was originally described by Begét and Hawkins (1989) from Alaskan loess. Following this study, magnetic enhancement due to wind vigour has been reported from various loess regions (Chlachula et al., 1998; Wang et al., 2006; Krevchinsky et al., 2008). Notably, Chlachula et al. (1998) found the characteristics of wind-vigour enhancement in Siberian loess. Wind-vigour enhancement is rare in the European Loess Belt, except for the cases reported in Zeeden et al. (2018) and Wacha et al. (2018). In both cases, the wind-vigour model is not the only process responsible for the magnetic enhancement but rather works in line with pedogenic processes.

Based on an analysis of Pampean loess, Bidegain et al. (2005) suggested the appearance of both pedogenic and wind-vigour magnetic enhancement in the same loess record. This phenomenon was further confirmed in Siberian loess, where Kravchinsky et al. (2008) found that while loess units display higher χ_{lf} than paleosol horizons, paleosols exhibit higher χ_{fd}, indicating mineral neoformation, such as ultrafine pedogenic magnetite/maghemite grains. A similar pattern was also reported by Wang et al. (2006) in the NE Tibetan Plateau and by Liu et al. (2012) in east Central Asia (Talede loess, Yili basin, Tianshan Mountains).

The recent study from Pegwell Bay loess (Stevens et al., 2020), also shows more complex control on the enhancement of magnetic susceptibility. Although significant increase of frequency dependent magnetic susceptibility was recognized by the increase of χ_{lf}, a significant discrepancy can be observed between the trend of Pegwell Bay and the "true loess line". Along with the pedogenic enhancement, the allocation of the data and its trend suggested the appearance of wind vigour enhancement in the "lower calcareous loess unit" (Stevens et al., 2020; p. 13).

2.2.2 Dissolution, magnetic depletion, and grain surface weathering

Along with the wind-vigour effect, relatively high χ_{lf} and low χ_{fd} compared to

typical loess, represented by the "true loess line", may indicate the dissolution of magnetic contributors by hydromorphic effects (Taylor et al., 2014). Particle dissolution due to waterlogging may affect ultrafine-grain single domain (SD) and small pseudosingle domain (PSD) particles before dissolving coarser multidomain (MD) magnetic particles. The dissolution of fine magnetic grains leads to a decrease in the concentration of ultrafine-grain components (e.g., the SP contributors responsible for χ_{fd}) and an increase in the mean magnetic grain size of the sediment (Taylor et al., 2014).

The effects of magnetic depletion also appear in the model of Zeeden et al. (2018), where the relatively low χ_{lf} but high χ_{fd} and $\chi_{fd\%}$ are driven by hydromorphic processes and/or intense weathering, as suggested by Baumgart et al. (2013). However, increasing ultrafine magnetic contributions cannot be described by hydromorphic processes, which, based on the theory of Taylor et al. (2014), would dissolve the finer components first and result in decreasing χ_{fd}.

Both wind-vigour and mineral dissolution effects result in relatively high χ_{lf} but low χ_{fd}. This begs the question of why some loess/paleosol layers in the ELB exhibit low χ_{lf} but high χ_{fd} (or χ_{fd}%) (Baumgart et al., 2013; Buggle et al., 2014; Maher, 2016; Zeeden et al., 2016, 2018). These phenomena appear in parts of loess profiles where the

pedogenic enhancement model can otherwise be applied: generally, loess yields comparatively lower χ_{lf} and χ_{fd} (χfd%: <5%), while the soil horizons have higher χ_{lf} and χ_{fd} (~10% or above) (e.g., Dearing et al., 1996). The appearance of enhancement trends different from the "true loess line" suggests that in addition to pedogenic enhancement, additional processes are operating.

Baumgart et al. (2013), supported by the model of van Velzen and Dekkers (1999), suggest that decreasing magnetic grain sizes caused by strong chemical weathering of larger primary particles is the cause of increasing χ_{fd} concurrent with relatively low χ_{lf} in paleosols. Chemical alteration as a possible cause of low χ_{lf} compared to relatively high χ_{fd} in Australian loess was also suggested by Ma et al. (2013).

One theory stems from observations by Wacha et al. (2018) of "detrital magnetic enhancement" in sediments from Susak (Croatia). In the study area, the trend of magnetic parameters of sandy loess displayed similar tendencies to paleosols (increasing χ_{lf} and χ_{fd}). Based on the magnetic experiments and observations of Buggle et al. (2014), Wacha et al. (2018) explained the "detrital magnetic enhancement" as a result of surface oxidation of the MD magnetic fraction and therefore formation of ultrafine SP grains on the surface of coarser detrital grains. A similar theory appeared in Zeeden et al. (2018), which suggests oxidation in source areas before the transportation

of dust to form loess. The oxidation of unweathered particles may create an oxidized rim consisting of ultrafine magnetic minerals around an unaffected core, resulting in higher χ_{lf} and χ_{fd} compared to unweathered particles (Buggle et al., 2014; Wacha et al., 2018).

The data from the "upper non-calcareous unit" of Pegwell bay loess (a profile with complex pattern of magnetic susceptibility enhancement) shows a shallower line of increased magnetic susceptibility parameter values compared to the "true loess line". This trend "may suggest some pedogenic enhancement but may also indicate hydromorphic alteration of magnetic minerals under redox conditions, leading to dissolution of magnetic particles (Stevens et al. 2020; p. 13).

2.3 Beyond the relationship between common magnetic susceptibility parameters

Although the focus of this study is the relationship between two commonly used magnetic susceptibility parameters, χ_{lf} and χ_{fd}, and their significance in the reconstructions of environmental processes, there are a great number of studies that concentrate on the magnetic mineral alteration and neoformation in loess paleosol sequences more widely, particularly focussing on goethite, magnetite, maghemite and hematite (e.g. Boyle et al., 2010; Jiang et al., 2018, and the references therein). Such

studies apply combined rock magnetic and geochemical (mostly diffuse reflectance spectroscopy – DRS) methods and have played a significant role in the understanding of magnetic enhancement of loess during pedogenesis, as summarised briefly below.

The early studies of combined magnetic and DRS research by Ji et al. (2001, 2002, 2004) contain the essential elements of this research line: redness (and other) colorimetric indices, the hematite/goethite ratio and the joint application of DRS and other climatic proxies. Following these first steps, Torrent et al. (2007) applied a combined rock magnetic and DRS method to describe the origin of various iron oxides, especially magnetite, maghemite and hematite and oxyhydroxide (goethite) in paleosols from the CLP. The proposed model concerning the pathway by which ferrihydrite is transformed into a transient maghemite-like phase before its final transformation into hematite was verified by the study of Hu et al. (2013). The study of Liu et al. (2011) verified the reliability of the DRS method in the quantification of the amount of hematite present and provided additional information about the potential bias in the method. Jiang et al. (2013) applied magnetic and DRS experiments and provided evidence concerning the aeolian origin of goethite in Chinese loess. The recent study of Jiang et al. (2018) provides a five-stage model about the magnetic mineral alteration (with a focus on magnetite, maghemite and hematite) in soil, which fundamentally

changes the conventional model by providing detailed steps and description of mineral alteration and neoformation, proposed by e.g. Barrón and Torrent (2002), Barrón et al. (2003), and Liu et al. (2008).

Although a great amount of combined rock magnetic and DRS studies attempting to understand the chemical pathways of pedogenic enhancement have been elaborated in Chinese loess, there is also some research on this on the ELB. Bábek et al. (2011) elaborated joint magnetic (e.g. magnetic susceptibility) and DRS study on Dolní Věstonice (Czech Republic) and Krasnogorskoye loess sections (SW Siberia, Russian Federation). The applied methods seemed to work well in the correlation of single successions, but the study also concluded that there is no universal proxy for weathering or pedogenesis intensity which can be applied across broad regions or along considerable climatic gradients (e.g., in continental scale). The observations of Bábek et al. (2011) raise some concern about the application of various magnetic and non-magnetic proxies and models in the case of various types of paleosols and continental scale correlations based on magnetic susceptibility. Paleosols, developed under paleomonsoon climate characterized by significantly higher precipitation might show different weathering characteristics and different degree of (magnetic) mineral alteration than the paleosols edeveloped under Atlantic or continental climatic influence,

for example. In addition, the varying magnetic mineral composition of the parent material of the soil (i.e. loess) may impact the magnetic mineral composition of soils (e.g., in some cases higher concentrations of hematite may appear in loess; Bradák et al. 2019a).

3. Materials and methods

3.1 Material

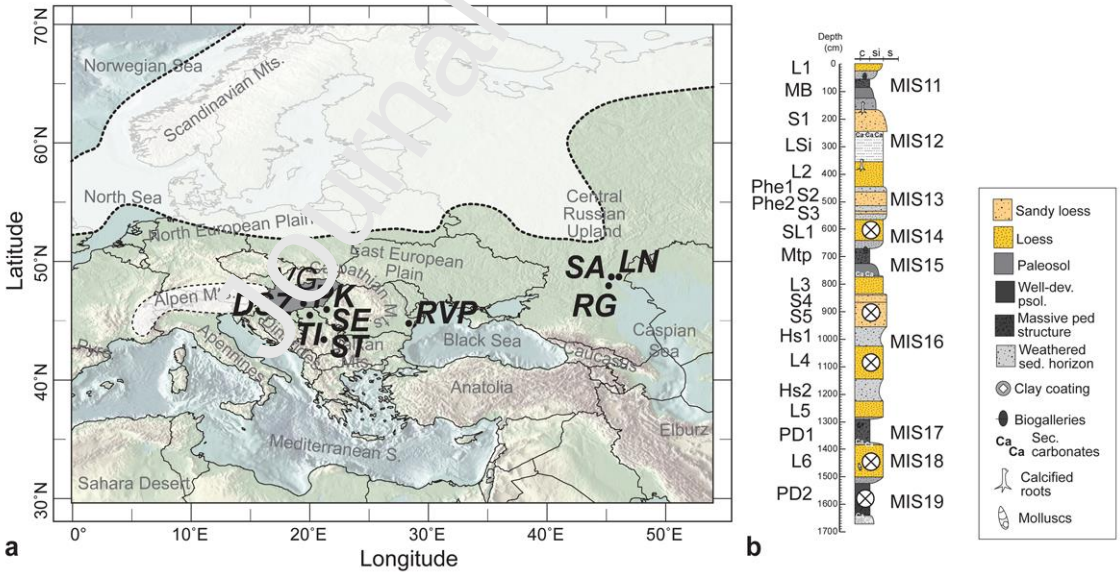

Figure 1. The geographical location of the Paks profile (Hungary) and other successions where magnetic parameters were analysed in this study (a) and the studied sequence with sampled units of the Paks loess-paleosol sequence (b). The abbreviations

of the profiles are as follows: Dunaszekcső - DSZ, Leninsk - LN, Paks - PK, Raigorod - RG, Rasova-Valea cu Pietre – RVP, Srednaya Akhtuba – SA, Stalać section – ST, Semlac – SE and Titel – TI loess. The circles with crosses indicate the sampling points for rock magnetic and SEM measurements from the Paks profile. The abbreviations of stratigraphic units in the Paks record are as follows: L1-6 loess, SL1-sandy loess; S1-5 very fine sand, MB – Mende Base paleosol, Phe1, Phe2 - Paks sandy soil complex, Mtp - hydromorphous soil at Paks, Hs1 and 2 – weathered sandy loess horizons, PD1 - Paks Double 1 paleosol, PD2 - Paks Double 2 paleosol. Detailed information about these units can be found in Bradák et al. (2019a and b) and in Supplementary Material 1. The boundary of glacial ice sheets in the study area was reconstructed using the works of Toucanne et al. (2009) and Batchelor et al. (2019). The basic relief map is from Amante and Eakins (2009).

The Paks loess profile is located to the north of the town of Paks in the Pannonian Basin, Hungary, on the right bank of the Danube River 46°38`24``N and 18°52`24``E, top of the sequence: ~135 m a.s.l.; Fig. 1a) (Újvári et al., 2014). The glacial deposits, corresponding to marine isotope stage (MIS) 18, MIS16, MIS14, MIS12 and MIS10, are represented by various aeolian sedimentary units (loess - L, sandy loess - SL, and

fine sand - S) in the studied section at Paks (Suppl. Mat. 1a, b and c). Interglacial deposits (MIS19, MIS17, MIS15, MIS13 and MIS11) are represented by various paleosols intercalated with sediment units such as PD2, PD1, Hs1-2, Mtp, Phe2-1 and MB (Újvári et al., 2014; Marković et al., 2015) (Fig. 1b; Suppl. Mat. 1d, e, f and g). As part of a recent sampling session for a detailed magnetic study at Paks, a 16-m thick loess/palaeosol sequence was cleaned and sampled (Fig. 1b). Block samples were taken every 10 cm. From each block, approximately 5 to 10 pieces of 2-cm^3 cube samples were prepared for further analysis (sum. 950 samples) (Fig. 1b). Detailed information about the units of the sampled section can be found in Bradák et al. (2018a, b and 2019a, b and Suppl. Mat. 1). The mass of the samples was used to compare the magnetic enhancement characteristics of the studied section in Paks loess with various loess successions from the ELB (Fig. 1a). Magnetic susceptibility data were collected and used from Költringer et al. (2020), Marković et al. (2011), Obreht et al. (2016), Újvári et al. (2016), and Zeeden et al. (2016, 2018). The abbreviations of the datasets (profiles) used in the manuscript are the following: Dunaszekcső - DSZ, Leninsk - LN, Paks - PK, Raigorod - RG, Rasova-Valea cu Pietre – RVP, Srednaya Akhtuba – SA, Stalać section – ST, Semlac – SE and Titel – TI loess (Fig. 1). Due to the nature of the study, i.e., focusing on the magnetic enhancement trends and the comparison of the applicability of

the “true loess line” in various successions, no detailed vertical characterization of the magnetic proxies from the Paks profile was executed. Such analysis can be found in Bradák et al. (2018a, b and 2019) and will be published in further studies in the near future.

Along with the samples used for susceptibility measurements, pilot samples were collected from various sediment layers of the Paks (PK) sequence, including the SL1, S5, L4 and L6 sediment units and PD2 paleosol horizon (Fig. 1b). These pilot samples represent aeolian loess (L4 and L6) and paleosol (PD2) horizons and units with uncommon magnetic susceptibility parameters, such as low χ_{lf} but relatively high χ_{fd} (SL1 and S5).

The material of L6 went through further preparation to reveal additional information about the magnetic enhancement of sediments. The aggregates appearing in loess were disintegrated by an ultrasonic bath. The finest clay contributors were separated from the coarser grain (silt and sand) mixture by a laboratory centrifugal separator (MLW Centrifuge T 52.1; Labexchange, Germany). Following the removal of clay components, the material of L6 was separated into two components by a strong magnet, placed into a plastic tube and immersed in the suspension for 24 hours. After removing the magnet from the suspension, the strong magnetic components of L6,

attached to the wall of the plastic tube, could be collected separately (Suppl. Mat. 2). This "extract" (EXT) mainly contains ferromagnetic minerals. The residual (RESID) was further separated into two groups by a sieve: a finer, mainly silt and fine sand grain size group (<125 μm; RESIDf) and a coarser sand grain size group (>125 μm; RESIDc). From the magnetic mineral point of view, RESID groups mainly contain dia- and paramagnetic components (e.g., phyllosilicates; Suppl. Mat. 2).

3.2 Methods

The low frequency (~0.5 and ~0.9 kHz) and high frequency (~4 and ~16 kHz) magnetic susceptibilities of ~2-cm^3 Paks samples were measured in the laboratory using an SM 100 portable susceptibility meter (ZH-Instrument, Brno, Czech) (Suppl. Mat. 3 and 4). Please note that for the SM 100, the sensitivity is ~5 × 10^{-6} SI units at 0.5 kHz and 1 × 10^{-6} SI units for 4 and 16 kHz frequencies.

To determine χ_{fd}, the susceptibility of the samples was measured at low and high frequencies. Absolute (χ_{fd}) and relative frequency dependence of magnetic susceptibility ($\chi_{fd\%}$) were used in environmental magnetic studies. The former is defined by the following:

$$\chi_{fd}=\chi_{lf}-\chi_{hf} \quad (1)$$

which was used in this and numerous previous studies (e.g., Dearing et al., 1996; Zeeden et al., 2016 and the references therein). χ_{fd} is a strongly operating frequency-dependent parameter (e.g., Hällberg et al., 2020), therefore, Hrouda (2011) proposed the use of χ_{fd} normalized by the differences of the natural logarithm of the applied high and low frequencies:

$$\chi_{fs} = (\chi_{lf} - \chi_{hf})/(\ln f_{hf} - \ln f_{lf}) \quad (2)$$

where χ_{fs} is the normalized χ_{fd}, and f_{lf} and f_{hf} are the low and high frequencies used during the experiments, respectively.

The use of χ_{fs} allows us to compare previously measured magnetic susceptibility data from various profiles obtained by different instruments. Since early studies in frequency-dependent magnetic susceptibility analysis of loess, there has been significant technical development in instrumentation, resulting in a wide range of applicable frequencies and sensitivities. As a result of such technical development, the widely used χ_{fd} and $\chi_{fd\%}$ parameters are biased by the various measuring frequencies that differ

between instrument models This bias or difference must be considered during the comparison of results from various profiles measured by various instruments. The normalization process suggested above provides a way to address such bias and makes data from various origins comparable. Following the calculation of χ_{fs}, a χ_{lf} and χ_{fs} plot can be used to characterize the relationship between the χ_{lf} and χ_{fs} of sediment and paleosol samples. The background susceptibilities were determined following the method of Panaiotu et al. (2011) by using the normalized frequency dependence of magnetic susceptibility. Background magnetic susceptibility represents the magnetic susceptibility of sediments without any pedogenic enhancement, i.e., without the influence of neoforming pedogenic magnetic components (Table 1 and Suppl. Mat. 4).

To estimate the domain state of magnetic components, hysteresis measurements were conducted using a Micromag 2900 AGM with an alternating gradient field magnetometer (Princeton Measurements Co.) and variable field translation balance (VFTB, Mag Instruments UG, Germany) (Suppl. Mat. 3 and 4). A maximum applied field of 1 T (the limitation of both instruments) was used for the hysteresis measurements. During the hysteresis measurements the following settings were used for Micromag AGM: field range - ±1 T, moment range - 200×10^{-9} A, averaging time - 100×10^{-3} s; and for the VFTB: dwell time - 1s, and data cycles and wait cycles - 15 s

and 10 s.

The coercivity of remanence (remanent coercive force) to coercivity ratio (Hcr/Hc) and saturation remanence to saturation magnetization (Mrs/Ms) plot, the so-called Day plot analyses (Day et al., 1977; Dunlop, 2002), were used to reveal the multidomain, single-domain (SD), superparamagnetic (SP) and pseudo-single domain (PSD) (in later studies: SD + MD mixture; Dunlop, 2002; or vortex state [VS]; Roberts et al., 2017) state of the magnetic mineral components in the samples (Suppl. Mat. 3 and 4).

Thermomagnetic experiments (temperature dependence of magnetization) were also carried out by VFTB from room temperature (~20-25 °C) up to 700 °C in air. The following parameters were applied during the thermomagnetic experiments: dwell time - 1s, dwell field - 35mT, ramp slope - 30 °C/min, data cycles - 10 s, and wait cycles - 2 s. Temperature variation in magnetization provides information about the transformation, e.g., the Curie temperature (Tc) of magnetic mineral components identifies the change in magnetic moment at different temperatures during heating and cooling (Suppl. Mat. 3 and 4).

The results of rock magnetic measurements were analysed by RockMagAnalyzer1.1 software (Leonhardt, 2009). During the analysis of hysteresis curves, all parameters were corrected using their dia- and paramagnetic fractions.

Loess, the extracted and residual samples were studied by using a JSM-6480LAII scanning electron microscope (SEM; JEOL, Tokyo, Japan) equipped with energy-dispersive X-ray spectroscopy (EDS), and a JXA-8900 electron probe microanalyser (EPMA) with a wavelength-dispersive X-ray spectrometer. Although magnetic extract from loess has been studied by SEM (e.g., Hyodo et al., 2020), to the best of our knowledge, this is the first time when experiments are made on the non, (or weakly) magnetic residual material. To obtain flat and smooth surfaces, we impregnated the samples with a low-viscosity resin (Petropoxy 154) and polished them using SiC and Al_2O_3 abrasives without lubricant to avoid alteration of clay minerals. For SEM observations, we used back-scattered electron imaging. Chemical analyses using EDS were obtained at 15 kV and 0.4 nA. Data corrections were made by the ZAF method with well-established natural/synthesized materials as chemical standards.

4. Results

4.1 Magnetic enhancement trends from ELB

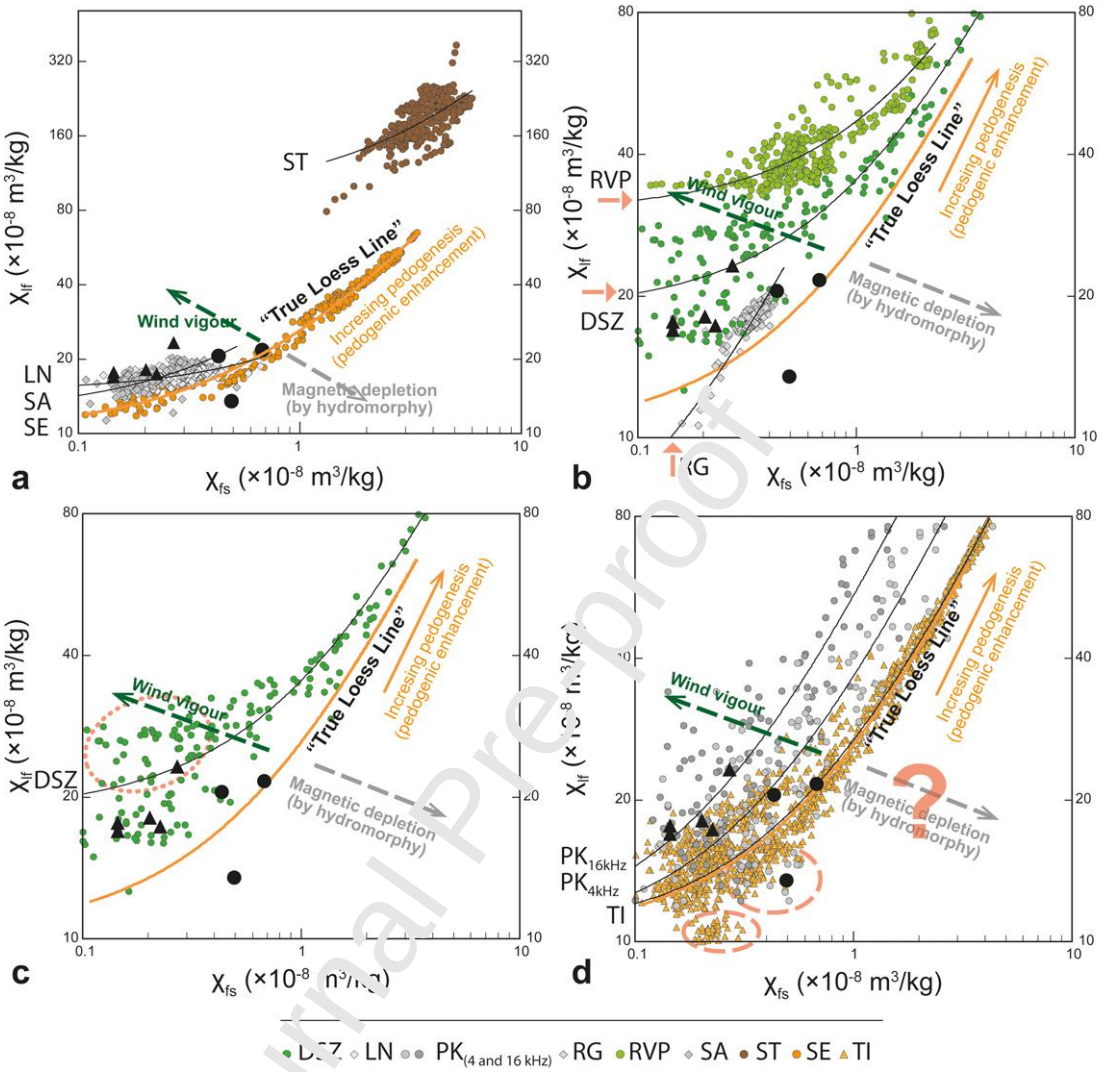

Figure 2. The complex magnetic enhancement model introduced by Maher (2011) and Zeeden et al. (2018). a) Samples with weak mathematical statistical relationships between the magnetic susceptibility parameters (LN, SA and ST) and the samples from the SE profile, characterized by the true loess line. b) Irregular background susceptibility (indicated by the red arrow for DSZ, RG and RVP). c) Discrepancy towards the "wind-vigour" region (red dotted circle) from the main magnetic enhancement trends (DSZ sequence). d) discrepancy towards the "magnetic depletion"

region (red dotted circle) from the main magnetic enhancement trends (PK and TI sequences). The triangles and circles indicate pilot samples from the PK site where EXT, RESIDf and c contributors were separated (triangles; see 2.1) for further magnetic analysis. The black circles represent sediment samples with irregular Hcr/Hc and Mrs/Ms values on Figure 4. The sources of magnetic susceptibility data are Költringer et al. (2020), Marković et al. (2011), Obreht et al. (2016), Újvári et al. (2016) and Zeeden et al. (2016, 2018).

A set of χ_{lf} and χ_{fs} data from various profiles of the ELB were used to verify the existence of the "true loess line", the trend of magnetic enhancement of aeolian sediments by pedogenic processes (Zeeden et al., 2018) (Fig. 2). Most of the data from profiles of various regions exhibit a positive correlation between χ_{lf} and χ_{fs} (average correlation coefficient r_{AVG}: 0.89), which suggests the pedogenic enhancement of magnetic susceptibility by SP particles. Low correlation coefficients among the studied sections were found at SA ($r = +0.56$, $p(a) < 0.05$, $n = 103$), LN ($r = +0.57$, $p(a) < 0.05$, $n = 315$) and ST ($r = +0.67$, $p(a) < 0.05$, $n = 410$) (Table 1; Fig. 2a). In some loess profiles, namely, RVP, DSZ and RG, the trend of magnetic enhancement was similar to the "true loess line" (increasing χ_{lf} and χ_{fs}), but significant deviations were observed in

the background susceptibilities (RVP, DSZ and RG) and due to data scatter (e.g., PK) (Table 1; Fig. 2b).

Differences in the background susceptibility of loess have been recognized for the DSZ (18.6×10^{-8} m^3/kg) and RVP (30.3×10^{-8} m^3/kg) sediments, where significantly higher background susceptibility is observed compared to the average 13.04×10^{-8} m^3/kg and median 10.03×10^{-8} m^3/kg values. In contrast, significantly lower background susceptibility was found in the RG section (4.4×10^{-8} m^3/kg) (Table 1; Fig. 2b, red arrow).

Increased scattering of data appears in samples with low χ_{lf}, for example, PK loess. Sediment samples with χ_{lf} values below ~40×10^{-8} m^3/kg exhibit a less significant relation between paedogenic enhancement (scattering χ_{fs}) and bulk magnetic susceptibility (χ_{lf}). This is seen in the scattered data distributions observed for the DSZ and PK sections (Fig. 2c and d). These samples are characterized by 1) relatively high χ_{lf} and low χ_{fs} compared to others (e.g., DSZ; Fig. 2c, dotted line circle) or 2) relatively low χ_{lf} but high χ_{fs} (e.g., PK and a group of samples from TI; Fig. 2d, dashed line circles).

Profile (ref); [n-number of samples]	Loess region	Equation of magnetic enhancement trend	r, [p(a)<0.05]	Backg. susc.

				(×10-8 m^3/kg)
Raigorod (RG; Költringer et al. 2020); [216]	East European Plain	y = 39.87x + 4.3659	0.93	4.4
Paks (PK) (4 kHz); [141]	Middle Danube Basin	y = 26.532x + 10.04	0.95	10.0
Paks (PK) (16 kHz); [141]	Middle Danube Basin	y = 44.219x + 10.04	0.95	10.0
Semlac (Se; Zeeden et al., 2016); [215]	Middle Danube Basin	y = 15.846x + 10.294	0.99	10.3
Titel composite section (TI; Marković et al., 2011); [1229]	Middle Danube Basin	y = 16.291x + 10.383	0.99	10.4
Srednaya Akhtuba (SA; Költringer et al., 2020); [103]	East European Plain	y = 19.695x + 12.296	0.56	12.3
Leninsk (LN; Költringer et al., 2020);[315]	East European Plain	y = 8.0712x + 14.882	0.57	14.9
Dunaszekcső (DSZ; Újvári et al., 2016); [315]	Middle Danube Basin	y = 16.944x + 18.561	0.99	18.6
Rasova-Valea cu Pietre (RVP; Zeeden et al., 2018); [348]	Lower Danube Basin	y = 16.67x + 30.333	0.90	30.3
Stalać (ST; Obreht et al., 2016); [410]	Lower Danube Basin	y = 25.111x + 93.001	0.67	93.0

Table 1. Summary of the magnetic enhancement trends in the studied sections of the ELB. Beyond recent magnetic measurements from Paks, other magnetic susceptibility data are collected from Költringer et al. (2020), Marković et al. (2011), Obreht et al. (2016), Újvári et al. (2016) and Zeeden et al. (2016, 2018).

4.2 Rock magnetic characteristics of PK loess samples

Rock magnetic and SEM analyses were conducted on selected PK samples located

in the region, which display significant scatters in the χ_{lf} vs. χ_{fs} plot (Fig 2, black triangles and dots).

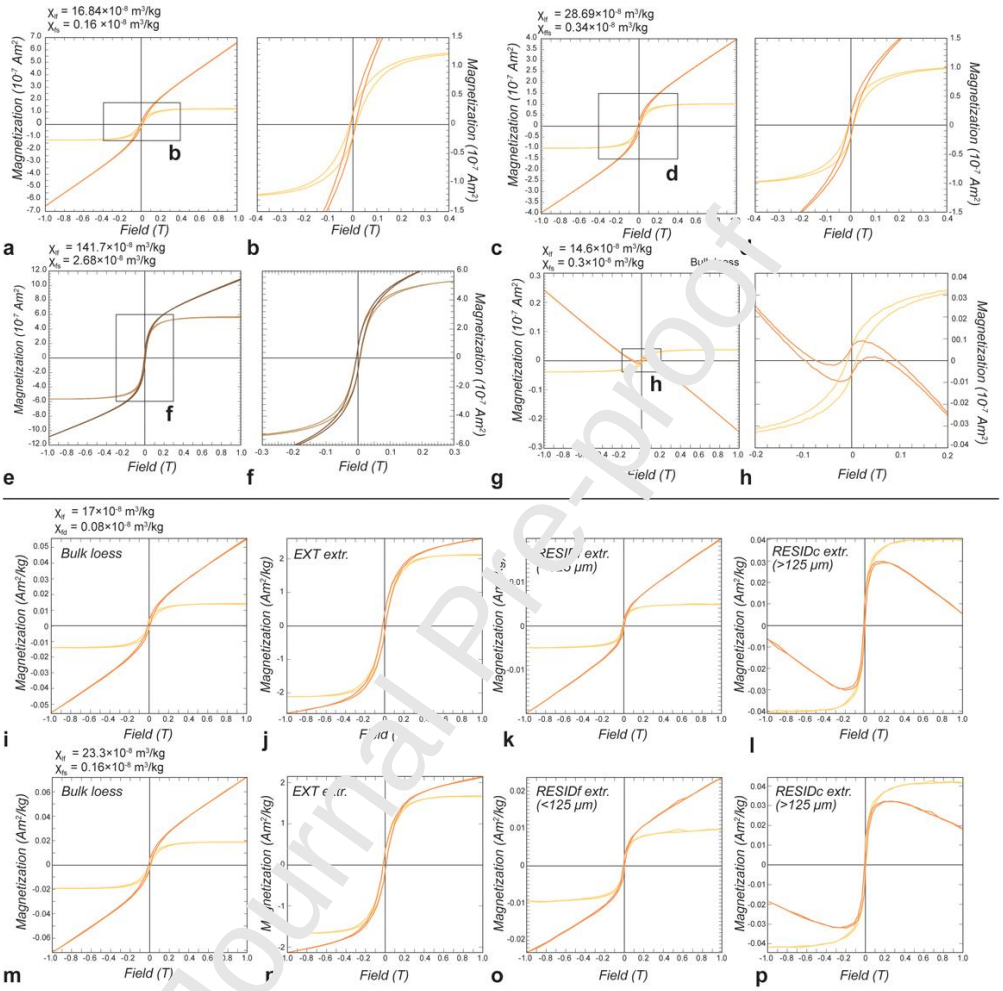

Figure 3. Comparison of hysteresis curves of aeolian, non-weathered loess (a-d), a well-developed paleosol horizon (e and f), and an aeolian loess unit with low χ_{lf} but relatively high χ_{fs} (g and h) compared to the normal range χ_{fs} of loess (Fig. 2d; sediment samples located close to the trendline of the "true loess line" and samples in the lower right area of the plot, indicated by dashed lines). The orange and dark brown curves

indicate the noncorrected values, and the yellow and light brown curves indicate the hysteresis loop after para- and diamagnetic correction. The hysteresis curves starting at panel i) display the results from bulk, EXT and RESID samples; bulk loess samples before extraction (i and m), EXT (j and n), RESIDf (k and o) and RESIDc (l and p).

The hysteresis curves of the selected samples from PK loess, characterized by a low χ_{lf} and variable χ_{fs} (Figs. 3a-d), are very similar to those of the paleosol sample from PK (Figs. 3e and f). An unusual hysteresis loop was identified in one sample from the PK section with a high χ_{fs} and one of the lowest χ_{lf} values; the presence of diamagnetic material with ferrimagnetic contribution is revealed by the appearance of a ferrimagnetic loop in the diamagnetic hysteresis curve (Fig. 3g and h). Similar hysteresis curves were also identified during the study of RESIDc (Fig. 3l and p).

The hysteresis loops of the loess sample closed at higher fields than the paleosol curve (Fig. 3a-f, i, j, m and n). This phenomenon can relate to a higher coercivity (antiferromagnetic) component in loess (Necula and Panaiotu, 2012).

The ratio of coercivity of remanence (remanent coercive force) to coercivity (Hcr/Hc) ranges from approximately 2.2 to 4.0 for all samples, with some values of approximately 5. The ratio of saturation remanence to saturation magnetization

(Mrs/Ms) ranged from approximately 0.11 to 0.17 for all samples, along with irregular values such as ~2 and 2.7 (Fig. 4). Based on the study of Dunlop (2002), such Mrs/Ms and Hcr/Hc ratios may indicate increasing amount of SD (and SP) contributors in the sediment samples, characterized by low χlf, but high χfs (Fig. 1, and 4).

Bulk loess samples and some of the RESIDf samples are in the region defined by Hcr/Hc: ~3-3.8 and Mrs/Ms: ~0.11 to 0.18 values). This region overlaps with that of loess samples from the CLP (Fukuma and Torii, 1996). Based on the improved Day plot (Dunlop, 2002), the samples fall into the region of the mixture of MD and SD grains (previously defined as PSD), with 15-25% SD content (Fig. 4). EXT and RESIDc samples contain slightly higher relative amounts of SD contributors (ca. 20-30%), based on their Hcr/Hc: ~2-2.8 and Mrs/Ms: ~0.11 to 0.15 values (Fig. 4).

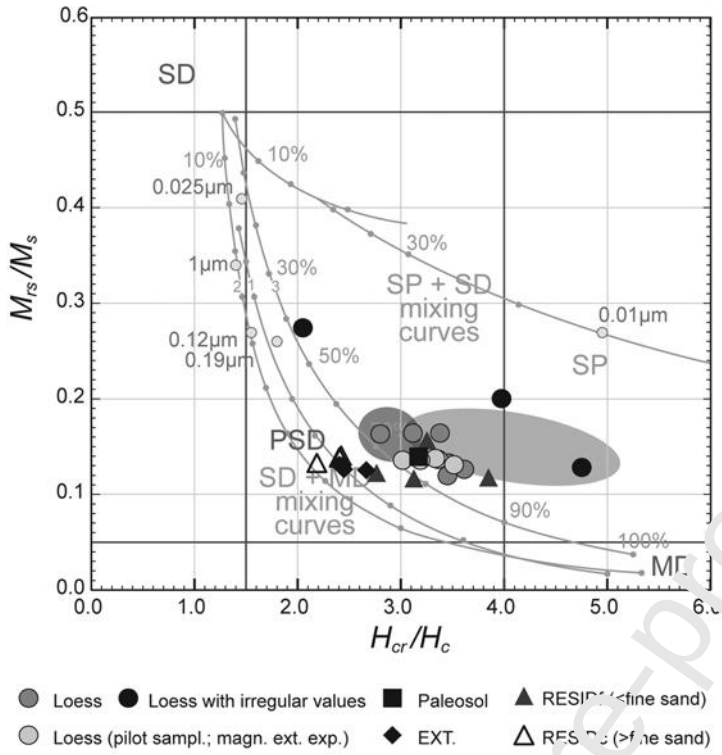

Figure 4. Magnetic domain (grain size) characteristics of the studied PK samples, revealed by Day plot analysis. The location of the samples indicates the characteristic magnetic domain (grain size) of the magnetic contributors. The PSD region indicates grains ~0.7 to 15 μm in diameter (magnetite; Nagy et al., 2019), the SD region indicates grains <0.7 μm (Nagy et al. 2019) and <15 μm (SD haematite; Dunlop, 1981), and the MD region indicates grains >15 μm in diameter (magnetite; Nagy et al., 2019). The light grey and dark grey areas represent the loess and paleosol samples from Xifeng, Chinese Loess Plateau (Dunlop, 2002).

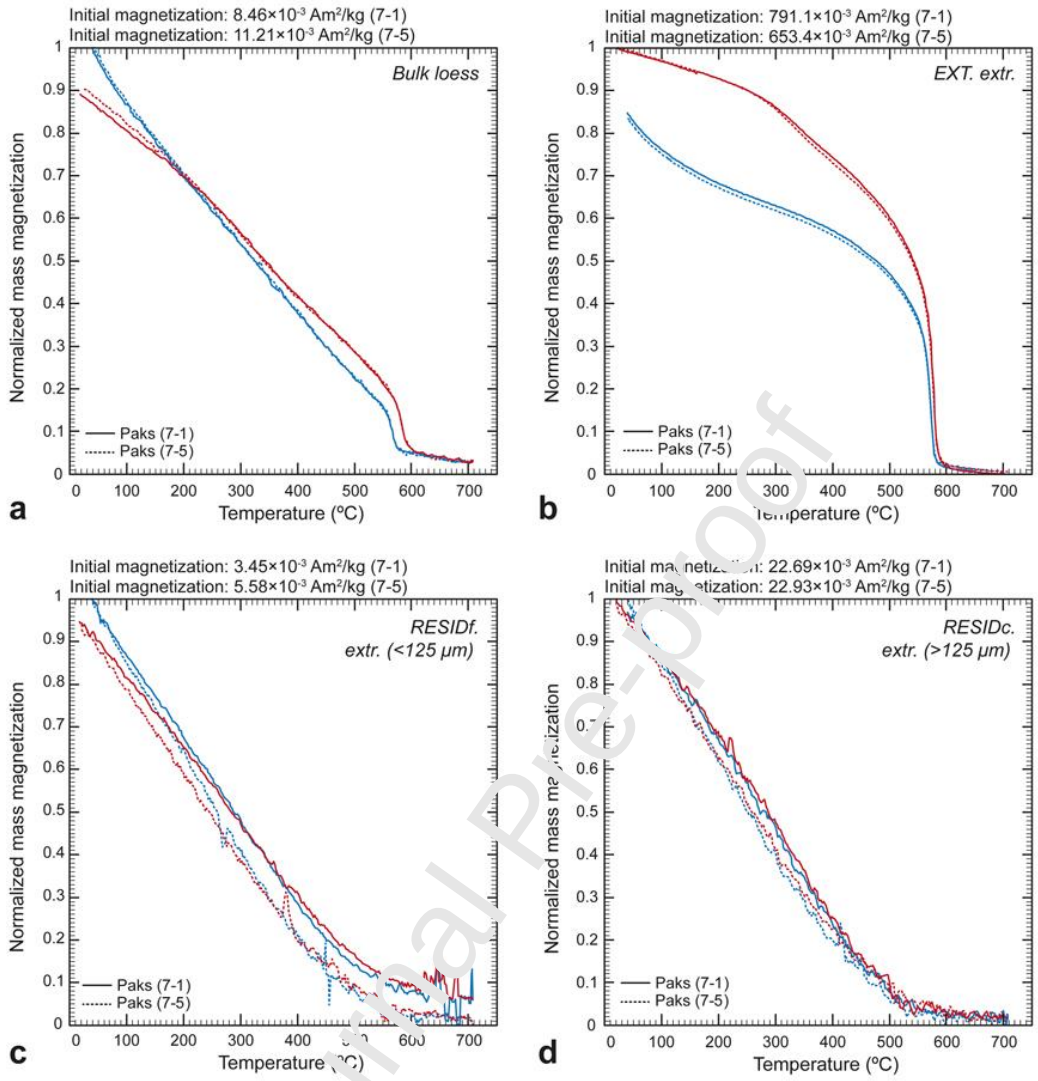

Figure 5. Results of thermomagnetic experiments on bulk loess (a), EXT (b), RESIDf, (c) and RESIDc (d) extracts. The red/blue curves indicate the heating/cooling phases.

Thermomagnetic analysis of bulk pilot samples from PK loess and on EXT and various grain size RESID extracts may allow the decomposition of the thermomagnetic curves of natural loess samples. The magnetization of bulk loess changes gradually until ~580 °C. Above ~580 °C, a drop in magnetization indicates the Tc of magnetite

(585 °C). There is still a weak magnetization above the Tc of magnetite, which may be related to haematite and fades with increasing temperature at approximately 700 °C (Fig. 5a). A hump was observed at ~250-300 °C on the heating curve of the EXT sample. In addition, an irreversible cooling curve (started about 560 °C) consists of a section below 200 °C where the cooling curve "crosses" the heating curve, and the initial magnetization is lower than the final magnetization after cooling to room temperature appears in bulk loess samples (Fig. 5a). It may indicate some mineral alteration during the experiment, which may occur above 200 °C. The hump and the irreversible cooling curve may indicate the conversion of thermally unstable maghemite (Gao et al., 2019). Compared to bulk loess, the most characteristic feature of the EXT heating curve is the drop around the Tc of magnetite (~580 °C) (Fig. 5b). Instead of this feature, which is completely missing in the thermomagnetic curves of RESIDf and c extract, the most characteristic feature is the gradual change of the magnetization (Fig. 5c and d). The gradual decrease in magnetization reaches near zero magnetization at approximately 500-550 °C and may reflect the blocking temperature of finer-grained (SD) (titano)magnetite (e.g., Day, 1975; Dunlop and Özdemir, 1997).

4.3 Binocular and scanning electron microscopy

Due to the possible appearance of very fine-grained magnetic contributors in loess identified by the magnetic methods above and some observed dark coloured patches on/in muscovite crystals during binocular microscope observation (Fig. 6a-c), SEM imaging was performed on the non-magnetic extracts, especially, but not limited to, muscovite minerals. The elemental map shows the appearance of submicron-level iron oxides along with Pb inclusions in muscovite (Fig. 6d and e).

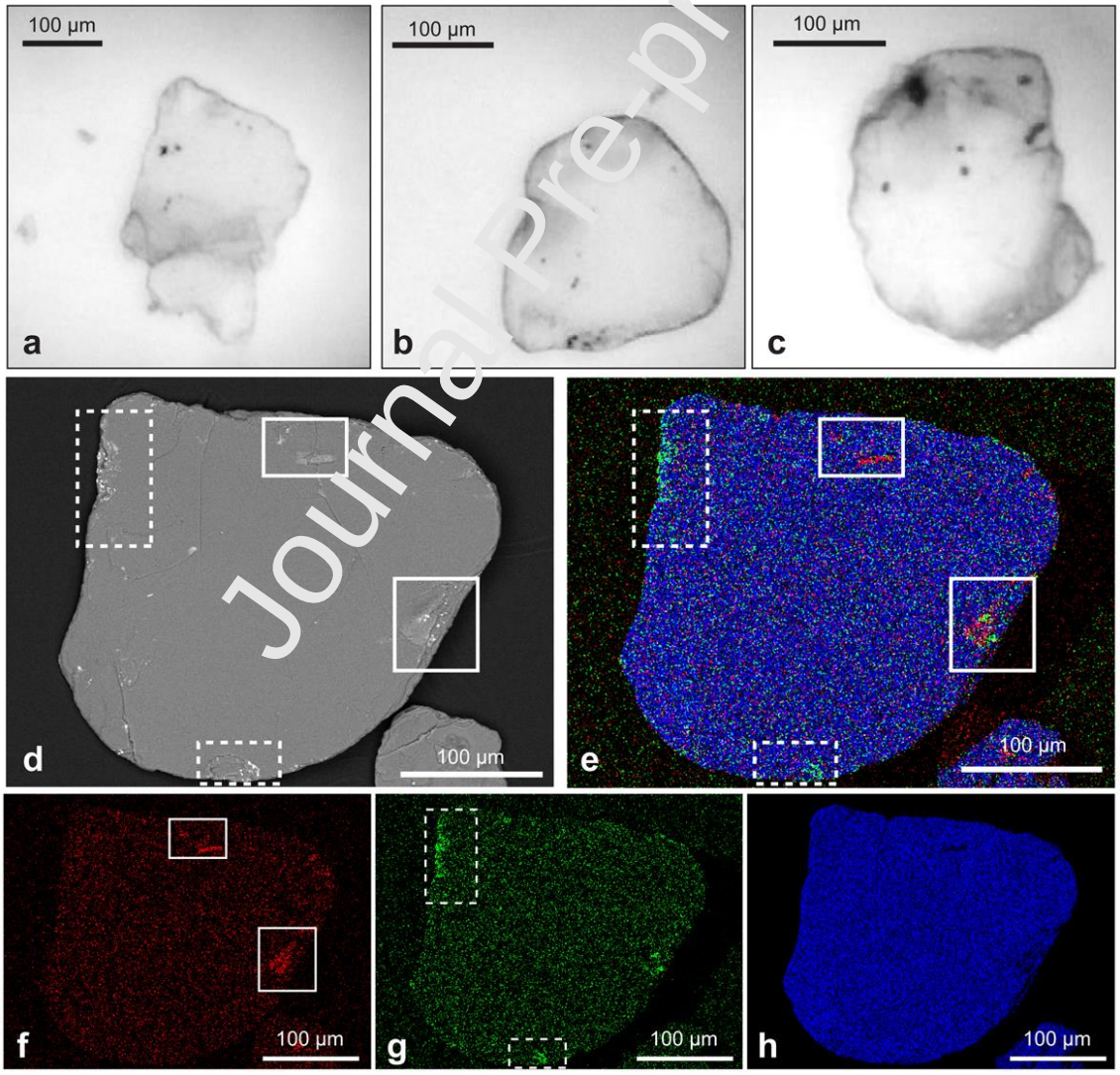

Figure 6. Binocular (a, b, and c) and scanning electron microscopy (d - backscattered

electron image and e - elemental scan image) images of muscovite grains from aeolian loess without any obvious sign of pedogenesis. The reddish areas denoted in solid line boxes indicate higher concentrations of iron. The greenish areas denoted by dashed line boxes indicate higher Pb concentrations, possibly related to galenite (PbS). Figure 6f, g and h are the corresponding element maps of the elemental scan image (Figure 6e), showing the Fe, Pb and Si element maps respectively.

The EDS from the areas of increasing Pb and Fe concentration (Fig. 7a, c and e) and from inclusions (Fig. 7b, d and f) both show a similar, but blended composition: although the components of muscovite(-chlorite) dominate the EDS, Pb and Fe peaks are also recognisable (Fig. 7). The mixed composition and the less characteristic appearance of the Pb and Fe peaks might be caused by the limitation of the instrument, which prevents us to reveal clear EDS of submicron size objects (e.g. the inclusions from Fig. 7b).

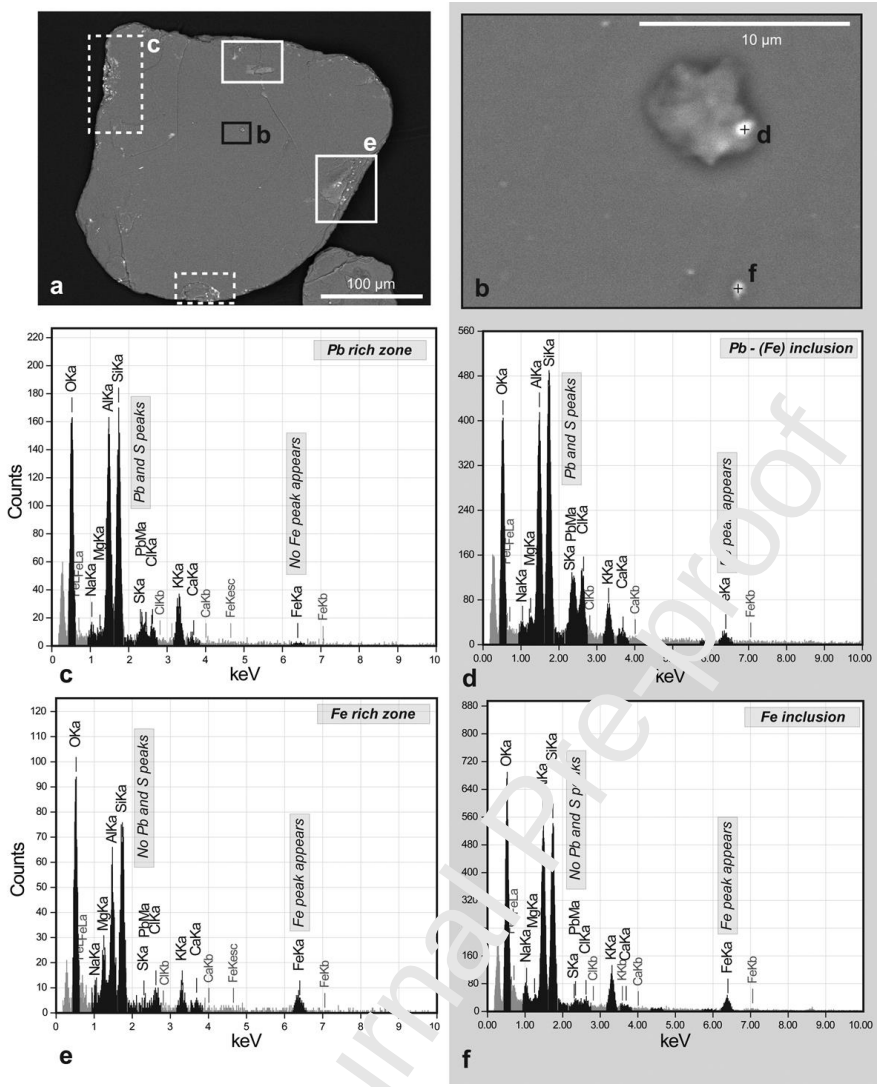

Figure 7. The characterization of the (magnetic) inclusions in muscovite from PK loess. a) One of the studied muscovite grains with regions characterized by increasing concentration of Pb and Fe (see Fig. 6d-h); b) surface and subsurface micron to submicron size inclusions in the grain; c and e) EDS representing the elemental composition of regions with increasing Pb (c) and Fe (e) content; and d and f) EDS of the inclusions, appearing on Figure 7b. The grey background connects the EDS related to the inclusions, observed in Figure 7b.

Signs of physical and chemical weathering on grains are also identified in the studied micrographs (Fig. 8) of sediment samples from the PK profile (characterized by low χ_{lf} and relatively high χ_{fs}). Submicron-sized, fragmented grains were found in sandy loess, possibly indicating physical weathering during deposition and diagenesis (Fig. 8a and b). Steps formed by conchoidal fractures (physical weathering) and partially altered by solution/precipitation structures (pits and channels) and coarse grains fully covered by a weathered surface can also be found in the same sediment unit (Fig. 8c and d).

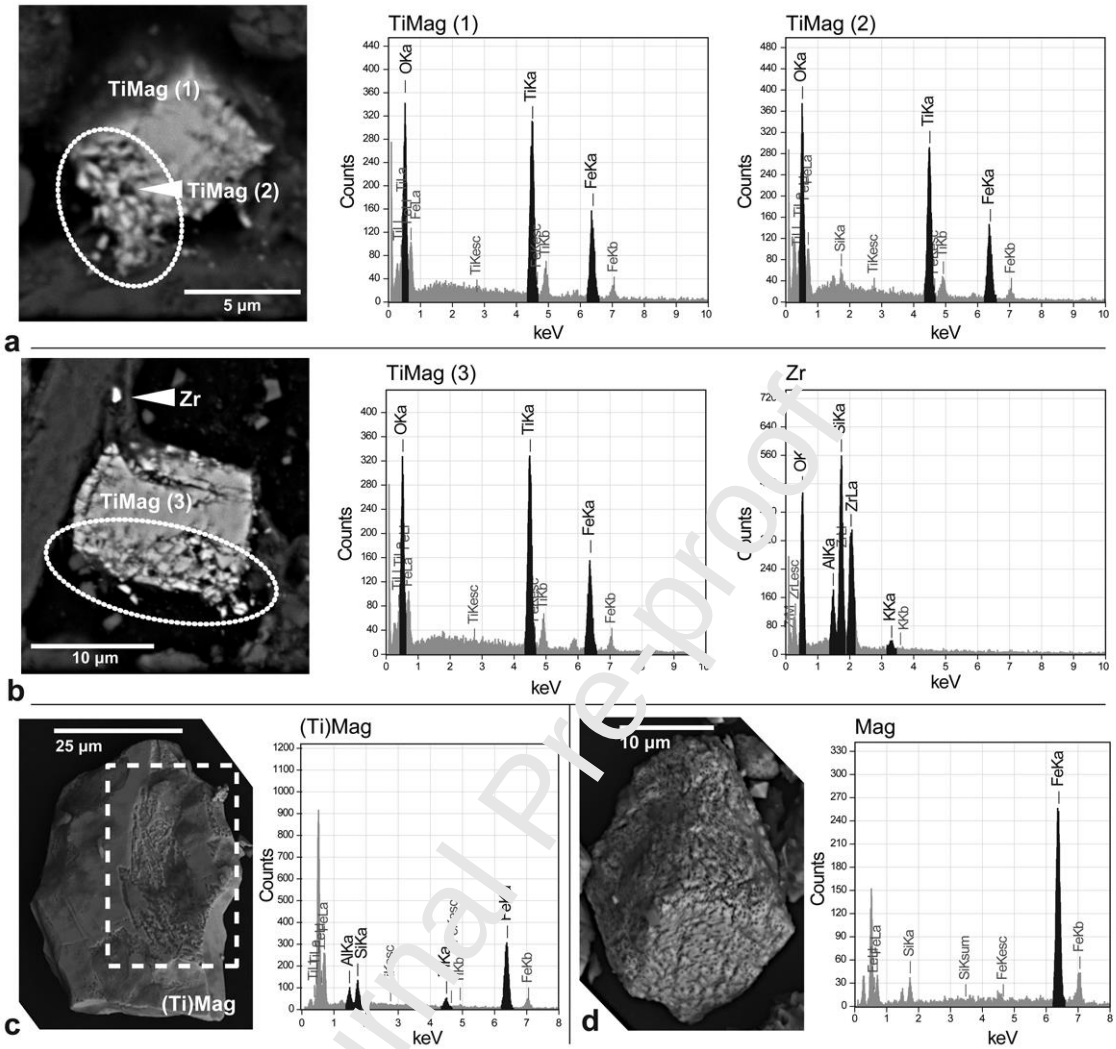

Figure 8. Nanofragmentation of titanomagnetite grains in samples from PK loess, indicated by low χlf and relatively high χfs (a and b). The areas marked by dotted line shapes demonstrate the physical weathering of the edge of coarser grains and the detachment of submicron size, fine-grain fragments. The effect of physical and chemical weathering on the grain surface (c). The area indicated by the dashed line box marks conchoidal fracture steps partially altered by solution/precipitation structures (pits and channels; more information about weathering marks in Vos et al., 2014, and Makvandi

et al., 2015). Example of magnetite with identical crystallographic planes but covered by pits (d), the sign of precipitation on the grain surface. Mineral types were identified by energy dispersive spectroscopy: Mag – magnetite, TiMag – titanomagnetite, and Zr – zircon.

5. Discussion

Figure 9. shows a summary of the key mechanisms (discussed in Section 5.1 and 5.2 in detailed) which may influence the enhancement of the magnetic susceptibility parameters during glacial-interglacial cycles. The "cycle of the enhancement of magnetic susceptibility" starts even before the transportation of dust. Differences in the magnetic parameters of the source materials of dust may cause significant differences in the magnetic susceptibility parameters of loess. The differences in the depositional environment (e.g. wind speed and interaction between grains) may influence the concentration and characteristic grain size of magnetic grains (Fig. 9; orange arrows). In contrast of the dry and arid dust depositional periods, chemical weathering may appear even during a slightly milder and humid periods, causing alteration on the surface of the particles. The influence of weathering (physical and chemical alteration, pedogenesis),

biogenic activity (e.g. formation of bacterial magnetite) and/or increasing (vertical) mineral migration and dissolution (e.g. in the body of the paleosol), triggered by the increasing precipitation and warmer temperature, is getting stronger during interglacial periods by during interglacial periods (Fig. 9; red arrows). The cycle of the enhancement of magnetic susceptibility signal restarts with the subsequent glacial period, following the interglacial with cooling, aridification and increasing dust accumulation (Fig. 9; blue arrows). As it is shown in Figure 9 and below in Section 5.1 and 5.2, processes, influencing the magnetic susceptibility parameter values in opposite way may appear parallel, causing complex magnetic enhancement. Therefore, the enhancement of magnetic susceptibility parameters cannot be described by one, exclusive model.

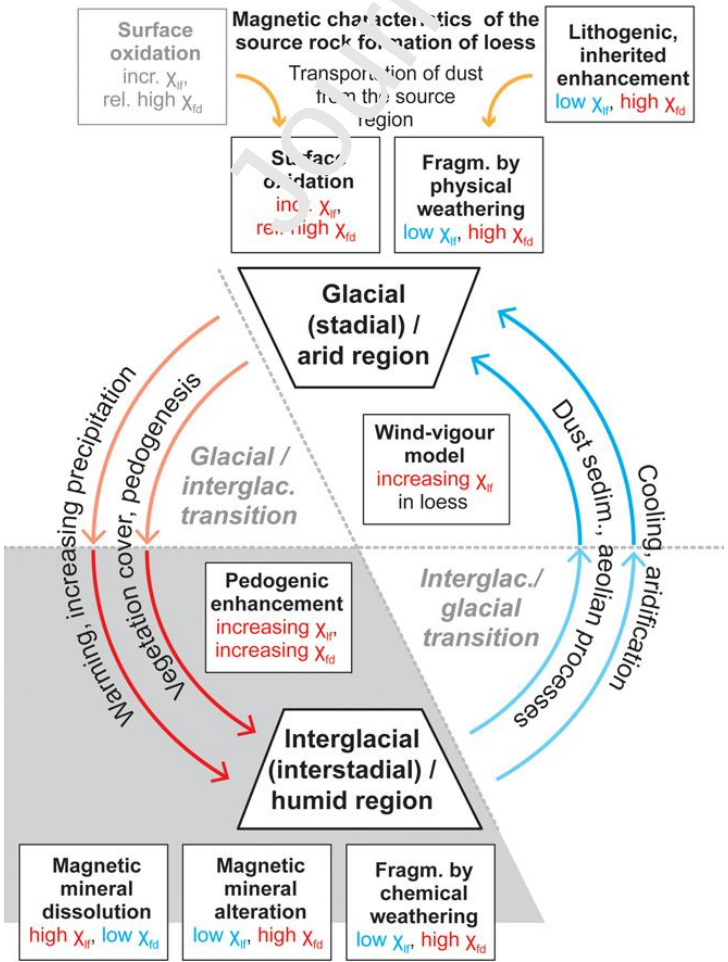

Figure 9. Cycle of the enhancement of magnetic susceptibility in loess and the summary of some key magnetic enhancement mechanisms in loess with an influence on χ_{lf} and $\chi_{fd(fs)}$ parameters during Quaternary glacial and interglacial periods. The grey region is characterized by increasing precipitation, temperature, pedogenic processes (red arrows) and intense chemical weathering. The blue arrows indicate cooling, aridification, increasing aeolian activity and dust accumulation. The yellow arrows mark dust transportation from the source area of loess. χ_{lf} and χ_{fd} are low field and absolute frequency dependent magnetic susceptibility, respectively.

5.1 Complexities in the the magnetic enhancement trend

The results above demonstrate that the pedogenic enhancement model explains the trends seen in most studied loess sequences (Table 2; Fig. 2) (e.g., Maher and Taylor, 1988; Heller et al., 1993; Forster et al., 1994; Dearing et al., 1996; Maher 2011, 2016; Zeeden et al., 2016, 2018). This implies that the amount of authigenic magnetic minerals increases during pedogenesis in the studied sediments (Fig. 2, Fig. 9). The pedogenic enhancement trends, observed, for example, in the SA, SE and TI successions, agree with this model. The trend lines and the allocation of the samples in

the χ_{fs} vs χ_{lf} plot of the LN, PK, RG, RVP and DSZ sections point to deviations (Fig. 2b, c and d; Fig. 9). The type of these deviations from the "true loess line" found in the characteristics of the enhancement trends and from the study of the relationship between χ_{fs} and χ_{lf} are summarized below (Table 2; Fig. 9).

Theories, models	Phenomena	Short description	Loess region	References (e.g.)
Pedogenic enhancement model	increasing χlf, increasing χfd	Magnetic enhancement of loess by in situ authigenic mineral forming during paedogenesis	CLP, ELB,	Heller et al. (1993); Maher et al. (1994, 2002, 2003); Panaiotu et al. (2001); Orgeira et al. (2011)
Wind-vigour model	low χlf in paleosols, high χlf in loess	Increasing input of dense magnetic particles by stronger, more frequent winds during glacial periods	Alaska, Siberia, ELB	Begét and Hawkins (1989); Chachula et al. (1998)
Lithological differences in the source area of the dust (theoretical)	low χlf in paleosols, high χlf in loess	Different source area of dust during glacial and interglacial periods	Pampean loess	Schellenberger et al. (2003)
Combined pedogenic and wind-vigour model	low χlf and high χfd in paleosols, high χlf in loess	The combination of the two main theories described above	Central Asia, CLP, ELB, Pampean loess, Siberia	Bidegain et al. (2005); Wang et al. (2006); Kravchinsky et al. (2008); Stevens et al. (2020)
Magnetic mineral dissolution	high χlf, low χfd	Dissolution of mainly fine-grain magnetic contributors by hydromorphic processes	ELB	Taylor et al. (2014)
Magnetic mineral alteration	low χlf, relatively high χfd	The gradual conversion of magnetite and maghemite to goethite in a humid environment (~940 mm/year)	Australian loess/parna	Ma et al. (2013)

Fragmentation by chemical weathering	low χlf, relatively high χfd	Destruction of coarse (detrital sedimentary) magnetic particles by strong weathering in paleosols	ELB	Bidegain et al. (2009); Baumgart et al. (2013); Gocke et al. (2014); Ghafarpour et al. (2016)
Surface oxidation ("detrital magnetic enhancement")	incr. χlf, relatively high χfd	Surface oxidation of coarse magnetic grains, and ultrafine magnetic mineral forming on their surface	ELB	Buggle et al. (2014); Wacha et al. (2018); Zeeden et al. (2018); Stevens et al. (2020)
Nanofragmentation (by physical weathering)	low χlf, relatively high χfd	Fragmentation of coarser sedimentary magnetic particles by physical processes during transportation and diagenesis	ELB	in this study
Lithogenic inherited magnetic enhancement, "lithogenic enh."	low χlf, relatively high χfd	Inherited fine-grain magnetic inclusions in phyllosilicates from the source rock of the dust	ELB	in this study

Table. 2. Summary of various magnetic enhancement models explaining the behaviour of χ_{lf} and $\chi_{fd(fs)}$ parameters in loess and paleosol units.

Based on the theory behind the pedogenic enhancement model, the statistical relationship between χ_{fs} and χ_{lf} is characterized by the r correlation coefficient. The r coefficient represents how strong the relationship is between the formation of fine-grain magnetic contributors (indicated by χ_{fs}) and χ_{lf}. In other words, a high r value may indicate that the enhancement is solely due to the neoformation of fine-grained magnetic contributors (e.g., SE and TI profiles). In contrast, low r values suggest 1) that the χ_{fs} and χ_{lf} values are similar, which means uniform paedogenic enhancement levels among

the units of succession; i.e. only one type of material (loess or paleosols, with quasi-uniform magnetic susceptibility parameters) appears in the studied section, or 2) a scattering of the data (see 4.1.2).

In the case of low r, the background susceptibility of the studied sequence, i.e., the parameter representing the susceptibility of non-enhanced sediment, may suggest specific processes having an influence on the χ_{fs} and χ_{pd} parameters. For instance, while ST sediments show a low r (r = +0.67, p(a) < 0.05, n = 410) together with extremely high background susceptibility (93×10^{-8} m^3/kg) the background susceptibilities of SA (r = +0.56, p(a) < 0.05, n = 103; 12.3×10^{-8} m^3/kg) and LN (r = +0.57, p(a) < 0.05, n = 315; 14.9×10^{-8} m^3/kg) are close to the average value (13.04×10^{-8} m^3/kg) characteristic of most sections (Table 1; Fig. 9). The low correlation coefficient associated with high background susceptibility in ST loess may indicate that the studied material is already strongly influenced by pedogenic processes (high pedogenic susceptibility) or originally the sediment itself has high detrital susceptibility compared with other studied sediments. SA and LN loess are characterized by low correlation coefficients associated with average background susceptibility, which suggests that no strong paedogenic enhancement appeared in the loess/paleosols of these sections.

Differences in the background susceptibility from the one defined by Zeeden et al.

(2016)`s "true loess line" can be observed in the RVP, DSZ, and RG profiles (Table 2; Fig. 2b, red arrows). For DSZ (18.6×10^{-8} m^3/kg) and RVP (30.3×10^{-8} m^3/kg), higher background susceptibilities are observed compared to the average value of 13.04×10^{-8} m^3/kg. These higher values probably represent detrital enhancement, i.e., the deposited dust originally had higher magnetic fractions. By contrast, significantly lower background susceptibility was found for the RG section (4.4×10^{-8} m^3/kg), potentially indicating a very low magnetic mineral content of dust or the depletion of magnetic contributors during sedimentation.

Greater scatter in the data was recognized in samples with low χ_{lf} (<~40×10^{-8} m3/kg) from DSZ and PK loess (Fig. 2). The scattering exhibits two characteristic patterns in the χ_{fs} vs. χ_{lf} plot (Fig. 2; Fig. 9): 1) low χ_{fs} but relatively high χ_{lf} (Fig. 2c, area separated by dotted oval) and 2) relatively low χ_{lf} but high χ_{fs} (Fig. 2d, area separated by dashed oval).

The *wind vigour effect* may be indicated by the scattered data of DSZ and RVP showing low $\chi_{fd(fs)}$ and relatively high χ_{lf} in loess (Fig. 2c; Fig. 9). It is likely that these factors reflect the increasing input of dense magnetic particles by stronger, more frequent wind gusts during glacial periods, similar to the cases from Alaska (e.g., Begét and Hawkins, 1989), Siberia (Chachula et al., 1998) and the European Loess Belt

(Wacha et al., 2018; Zeeden et al., 2018) (Table 2).

The less known or overlooked theory about relatively high χ_{lf} associated with low χ_{fs}, which appeared in DSZ and RVP loess, may be caused by the *dissolution of fine magnetic minerals* (Table 2). Chemical weathering (dissolution) of magnetic mineral components, preferentially starting with the finest magnetic mineral contributors, may be responsible for the significant decreases in the fine grain components of loess, causing decreasing $\chi_{fd(fs)}$ values (Taylor et al., 2014). However, this hypothesis may not apply to samples from, e.g., the DSZ sequence which have not experienced significant weathering reported from the sediment units (Újvári et al., 2016).

Among the studied sections, some samples with scattered PK data and a group of samples from TI show significant deviations from their main magnetic enhancement trends towards relatively increased χ_{fs} (Fig. 2, area marked by red dashed oval). There are some hypotheses that may describe such features (see below; Table 2; Fig. 9).

Bidegain et al. (2009) observed a lower χ_{lf} associated with an increasing χ_{fd} in Pampean loess (Argentina). They attributed this feature to paedogenesis, which resulted in the *weathering of coarser magnetic grains in the parent material* (i.e., decreases in χ_{lf}) but increases in the ultrafine-grained particles. Baumgart et al. (2013) reported high χ_{fd} associated with relatively low χ_{lf} in paleosols and attributed the phenomenon to the

effect of strong weathering on detrital magnetic particles. The observed "reversed trend of decreasing χ_{lf} with increasing χ_{fd} was considered as weathering of larger magnetic mineral grains" in Nussloch loess as well (Gocke et al., 2014; p. 307). The destruction of coarser magnetic grains may result in increasing χ_{fs} in the studied PK loess (Fig. 2d, area marked by red dashed oval), but chemical alteration can be ruled out (i.e., there are no signs of strong weathering or paedogenesis).

Similar to Baumgart et al. (2013), Ma et al. (2012) reported rather high χ_{fd} and low χ_{lf} from Australian aeolian deposits (Mackenzie's Waterholes Creek - MWC profile) and described the phenomenon as a result of *magnetic mineral alteration*. During chemical alteration, magnetite and maghemite gradually converted to more stable goethite in a humid environment (expected ~940 mm/year based on modern annual precipitation data), causing χ_{lf} to decrease (Table 2). In the Middle Danube Basin, approximately 200-350 mm/year annual precipitation is estimated during the sedimentation of loess, and even during the paedogenic periods, it might not have reached 700 mm/year (Panaiotu et al., 2001; Bradák et al., 2011). As such, strong weathering processes as the cause of unusual magnetic susceptibility parameters may be excluded in the case of PK and TI loess.

Buggle et al. (2014), Wacha et al. (2018) and Zeeden et al. (2018) proposed the

formation of ultrafine grains on the surface of coarser magnetic hosts by surface oxidation of MD magnetic grains as a cause of increasing χ_{fd} in sediments (i.e. "detrital magnetic enhancement") before the influence of pedogenesis (Table 2; Fig. 9). In the case of PK or TI loess, the likelihood of surface oxidation in coarser grains cannot be excluded or verified as a cause of increasing χ_{fs} from analysis of susceptibility alone; therefore, additional rock magnetic and SEM analyses were performed on samples from PK (see below in 4.2).

Dual processes, *the competing appearance of pedogenic magnetic enhancement and the wind-vigour effect*, may offer an alternative explanation for the low χ_{lf} (wind-vigour effect) and higher $\chi_{fs(fd)}$ (pedogenic enhancement). Such a combination of magnetic enhancement was observed in loess successions, e.g., in the Tibetan Plateau (Wang et al., 2006) and in Siberian loess (Kravchinsky et al., 2008) (Table 2), but due to the lack of any sign of pedogenesis in the mentioned samples from Paks, the case of "dual enhancement" can be excluded (Fig. 2).

5.2 Additional observations on the potential causes of increasing χ_{fs} in PK loess

5.2.1 Fine-grained magnetic contributors of PK loess

The formation of submicron-sized magnetic particles on the surface of coarser

magnetic grains may explain the increasing χ_{fs} in samples with low χ_{lf} from PK loess.

The magnetic domain size of both loess and paleosols from the PK site falls into the PSD or mixed MD and SD region (Dunlop, 2002) (Fig. 4). Similar to what was seen in the selected samples from PK loess (Fig. 4), analyses from Alaska (Lagroix and Banerjee, 2002), the CLP (e.g., Liu et al., 1992; Pan et al., 2002; Jin and Liu, 2010; Li et al., 2018) and ELB (e.g., Taylor et al., 2014; Necula et al., 2015) report that PSD or mixed MD and SD state (with 10-30% SD contribution) components are the main magnetic contributors both to loess and paleosol units.

The study of both bulk loess and separated EXT, RESIDf and c extracts from the same loess samples helps to uncover various ways of magnetic enhancement in sediments. RESIDc extracts, dominated by coarse grains (>125 μm; fine sand), are characterized by PSD (mixed SD and MD) character and show slightly higher (cc. 20-30%) SD contents than the natural samples (Day plot, Fig. 4). This observation suggests that coarser contributors may somehow be associated with ferrimagnetic grains, including SD grains in the RESIDc extract, which dominantly contain dia- and ferromagnetic minerals. The differences between the saturation magnetization of the non-corrected and corrected hysteresis loops indicate significant amounts of high coercivity/dia- and paramagnetic components in PK pilot samples (Richter and van der

Pluijm, 1994) (Fig. 3a-f). A high ratio of paramagnetic contributors may influence the magnetic susceptibility values as well. As suggested by Rochette (1987) and Hrouda and Jelinek (1990), for materials characterized by low magnetic susceptibility ($\kappa_{lfavg} < 5\times10^{-4}$ SI), the paramagnetic components contribute significantly to the low field magnetic susceptibility value. In PK loess, which consists of larger amounts of paramagnetic contributors compared to the ferrimagnetic components, a low susceptibility value may also suggest significant paramagnetic contributions. In addition to the influence of paramagnetic minerals on χ_{lf}, paramagnetic minerals (e.g., phyllosilicates) may function as a host of nanosized ferromagnetic inclusions as well (see below).

5.2.2 Potential signs of surface weathering, inclusions and "nanofragmentation"

The bulk samples from PK loess exhibit somewhat complex magnetic character, including significant paramagnetic, SD and MD, and mainly low coercivity (magnetically soft) contributors such as magnetite and maghemite (Figs. 3, 4 and 5). Such a complex magnetic character is similar to the general magnetic character of loess, reported from various loess regions (e.g., Maher, 2011, and the references therein). In addition, the following features in the thermomagnetic curves (Fig. 5) and in the SEM

micrographs may provide additional information about the magnetic enhancement of PK loess samples (Figs. 5, 6, 7 and 8).

1) Appearance of maghemite as a potential indicator of surface weathering. Along with coarser grained MD magnetite (indicated by its Tc at 585 °C, for example), the magnetic extract contains unstable maghemite, revealed by an inflection point (a bump) on the heating curve at approximately 250 °C, indicating its decomposition (Gao et al., 2019) (Fig. 5b). Maghemite seems to be a common contributor in loess-paleosol sequences, as it has been identified in loess (e.g., Evans and Heller, 1994; Liu et al., 2003; Liu et al., 2010; Bradák et al., 2018a, b) as well as paleosol horizons (e.g., Deng et al., 2000, 2001; Zhu et al., 2001; Gao et al., 2019).

Unstable maghemite forms by chemical alteration, which makes it a sensitive environmental proxy (Gao et al., 2019). Maghemite appearing in sediments may indicate weak weathering during a slightly warmer/wetter phase within the cold and dry sedimentation period in glacials (Stevens et al., 2020). However, an alternative explanation follows the detrital magnetic enhancement theory, as suggested by Buggle et al. (2014). This study proposes that the formation of fine-grained maghemite (PSD and SD grain size) on the surface of coarser grains occurs before/during the sedimentation of dust. Based on the rock magnetic study of loess, Spassov et al. (2003)

suggest the appearance of similar features in Chinese loess, i.e., loess detrital magnetite with a weathered crust of maghemite. Weathering and chemical alteration of the surface of coarser grains was observed on SEM images of PK loess, which may support the view of Buggle et al. (2014) or Gao et al. (2019) (Table 2; Fig. 8c and d).

2) Appearance of ferrimagnetic inclusions in para- and diamagnetic loess components. Hysteresis and thermomagnetic experiments on RESIDf and c extractions from loess samples from the PK sequence (especially coarse, muscovite dominant grains; >125 μm) reveal key information about the magnetic enhancement of sediments. The weak, gradual decreasing magnetization, which reaches zero below the expected Tc of magnetite, may indicate that SD grains of various sizes gradually reach their unblocking temperature (e.g., Day, 1975; Dunlop and Özdemir, 1997) (Fig. 5c and d). In addition, the hysteresis curve of those coarse-grained nonferromagnetic samples shows a somewhat complex pattern: a diamagnetic curve with a ferromagnetic loop (Fig. 3l and p). Similar hysteresis loops were also observed in some natural samples with low χ_{lf} and higher χ_{fs} in PK loess (Fig. 3g and h). This type of hysteresis loop is rare for loess; to the best of our knowledge, no similar case has yet been reported from loess profiles. The appearance of this curve suggests that the magnetic properties of the studied loess sample are mainly characterized by diamagnetic contributors, but ferrimagnetic

components may appear. The weak influence of the ferromagnetic contributors (and the increasing influence of para- and diamagnetic minerals) is already suggested by the very low χ_{lf} (see above at the end of 4.2.1, and in Rochette, 1987; Hrouda and Jelinek, 1990), but the following experiments were needed to reveal the nature of ferromagnetic components.

The similarities between these hysteresis loops of natural samples and RESIDf and c extracts (Fig. 3g-h, l and p) were explored further by SEM experiments. RESIDc extracts of loess (Fig. 6 and 7) showed diamagnetic hysteresis curves with ferromagnetic loop (indicating low-coercivity magnetic components), similar to natural samples (Fig. 3l and p). The SEM analyses also indicate the appearance of submicron-scale (≤0.5-0.6 μm) magnetic components (Figs. 6d, e and 7) in natural sediments as well as in RESIDc extracts. The elemental mapping of individual muscovite grains suggests that such components may appear as inclusions in coarser grain phyllosilicate carriers (Fig. 6d and e; Fig. 7) (Table 2).

Such inclusions have already been reported from well-developed paleosols as a result of in situ pedogenic mineral neoformation (Yang et al. 2013; Sano et al. 2017; Hyodo et al. 2020). The observation of ferromagnetic inclusions in muscovite from loess without the sign of pedogenesis supports an alternative mode of origin (Fig. 6 and

7). These identified nanosize components in sediments may be traced back to their primary source rock lithologies, formed during various lithogenic processes as inclusions, e.g., in micas ("lithogenic enhancement") (e.g., Dunlop et al. 2006). Following the physical weathering of the source rocks, the micas with ferromagnetic inclusions were transported from their provenance (in the case of PK, from the Alps and Carpathians) and from local sources, e.g., alluvial fans (Újvari et al. 2012; Thamó-Bozsó et al. 2014), during glacials and redeposited as loess sediments. Iron oxide inclusions observed in muscovite (Fig. 6e and 7) can be regarded as a potential source of "lithogenic enhancement" in the sediment(s) from PK. Along with magnetite, galenite inclusions may also appear (Fig. 6d, e and g), which are characteristic components in certain magmatic and metamorphic rocks (e.g., granite). In the region of Paks, there is a potential geological formation that contains a significant amount of galenite. In the so-called Velence Granite Formation (Velence Mts., W. Hungary; Fig. 1), galenite appears as a result of regional high-temperature fluid flow events of a hydrothermal system of Mid- to Late-Triassic age related to the regional heating of the granite (Benkó et al., 2014). These hydrothermal processes might also be responsible for the formation of iron-oxide inclusions (e.g., Nadoll et al., 2014). Following the weathering and erosion of the Velence Granite Formation, component minerals (e.g.,

muscovite) of granite containing galenite and magnetite would have been transported and redeposited in the Paks region as constituents of loess. This observation supports the study of Schellenberger et al. (2003), who emphasized the importance of lithological differences in the source area of the dust for magnetic enhancement.

3) Physical weathering and nanofragmentation of coarser grains. As suggested by Bidegain et al. (2009), Baumgart et al. (2013) and Gocke et al. (2014) (Table 2), strong chemical weathering of coarser magnetic contributors may cause relatively low χ_{lf} but increasing $\chi_{fd(fs)}$ in paleosol horizons of loess successions. However, weathering processes may not be limited to paleosol horizons and do not necessarily require conditions conducive to strong chemical weathering to fragment coarser grains, as shown in SEM micrographs (Fig. 8a and b). Based on the SEM observations of PK samples with no marks of strong chemical alteration, there is one more process that may form nanosize magnetic particles in the sediments: fragmentation during deposition (e.g., by the collision of grains) and during diagenesis (e.g., by compaction). The formation of nanosized fragments increases the χ_{fs} of the sediment, but the χ_{lf} (i.e., the concentration of magnetic contributors) does not change. The appearance of nanofragmentation in loess sediments may indicate increasing physical weathering during transportation associated with strengthening of the transport agent. The

strengthening of the wind and/or the forgoing fluvial processes before the aeolian "redeposition" results in the transportation of coarser grains and intensifies grain collision and fragmentation.

The three processes summarized above potentially influence the magnetic enhancement in the case of low χ_{lf} associated with high χ_{fs} in apparently unweathered loess. The mentioned processes may contribute to more robust palaeoenvironmental reconstructions in loess by, e.g., indicating weak weathering processes over short, moderate-to-humid periods during loess sedimentation (maghemitization) and marking "harsher" cold periods with the intensification of winds (nanofragmentation).

6. Conclusions

The two generally accepted models (pedogenic and wind-vigour) used to explain the enhancement of magnetic susceptibility parameters in loess apparently do not cover the full range of potential causes of magnetic enhancement in loess. Uncommon cases are indicated by "suspicious horizons", characterized by high background susceptibility, lower χ_{lf} but higher χ_{fs}, and vice versa.

Despite the popularity of magnetic susceptibility parameters and the growing number of irregular cases observed, knowledge about the causes of magnetic enhancement in loess is still limited. Combined scanning electron microscopy (SEM) and magnetic analyses suggest possible causes of increased χ_{fs} in non-altered sediments: the nanofragmentation of coarser grains and the appearance of significant amounts of fine magnetic inclusions in dia- and paramagnetic components, e.g., in muscovite.

Such nanoscale magnetic inclusions may originate from various igneous and metamorphic processes, which developed inclusions in phyllosilicates and appear as mineral components in the dust source rock ("lithogenic enhancement"). Following the physical weathering of the rocks containing the magnetically enhanced micas, the grains would be transported from their provenance to the loess regions and be (re)deposited as aeolian loess during glacial periods. Increasing transport energy may lead to the mobilization of coarser grains, rolling and bombardment of the surface. Crushing of coarser grains may lead to physical weathering and the formation of fine, submicron size components ("nanofragmentation").

The summary of the methods of magnetic enhancement of loess also showed that pedogenic processes do not always lead to enrichment in magnetic contributors but can cause dissolution and magnetic depletion of certain components. Such processes may be

dependent on the type of soils and the characteristics of the environment in which the paleosol formed.

The methods of magnetic enhancement recently discovered in loess may not challenge the significance of the basic models, as suggested earlier, but rather describe an unusual feature observed in loess successions that researchers should consider in their interpretations of magnetic susceptibility data.

Acknowledgements

We are thankful for Professor M. Hyodo (Kobe University, Japan) for the discussions and support, and Á. Carrancho and the Paleomagnetic Laboratory (University of Burgos, Spain) for facilitating the magnetic measurements.

B. Bradák acknowledges the financial support of project BU235P18 (Junta de Castilla y Leon, Spain) and the European Regional Development Fund (ERD), project PID2019-108753GB-C21 / AECI / 10.13039/501100011033 of the Agencia Estatal de Investigación and project PID2019-105796GB-100 / AECI / 10.13039/501100011033 of the Agencia Estatal de Investigación. Part of the measurements were conducted during a fellowship awarded to B. Bradák at Kobe University, Japan, by the Japan Society for the Promotion of Science (JSPS; P15328). Part of this study was conducted within the

cooperative research programme of the Center for Advanced Marine Core Research, Kochi University (15A001, 16A002, 17A016), with the support of the Japan Agency for Marine-Earth Science and Technology (JAMSTEC). The Swedish Research Council is gratefully acknowledged for funding to TS for part of this project (2017-03888).

We are also thankful for the inspiring ideas and comments of two anonymous reviewers.

References

Amante, C. Eakins, B.W. 2009. ETOPO1 1 Arc-Minute Global Relief Model: Procedures, Data Sources and Analysis. NOAA Technical Memorandum NESDIS NGDC-24. National Geophysical Data Center, NOAA. doi:10.7289/V5C8276M.

Batchelor, C.L., Margold, M., Krapp, M., Murton, D.K., Dalton, A.S., Gibbard, P.L., Stokes, C.R., Murton, J.B., Manica, A. 2019. The configuration of Northern Hemisphere ice sheets through the Quaternary. Nature Communications (2019) 10:3713, doi:10.1038/s41467-019-11601-2 | www.nature.com/naturecommunications

Bábek, O., Chlachula, J., Grygar, T.M. 2011. Non-magnetic indicators of pedogenesis related to loess magnetic enhancement and depletion: Examples from the Czech Republic and southern Siberia. Quaternary Science Reviews 30, 967–979.

doi:10.1016/j.quascirev.2011.01.009

Balsam, W.L., Ellwood, B.B., Ji, J., Williams, E.R., Long, X., El Hassani, A., 2011. Magnetic susceptibility as a proxy for rainfall: Worldwide data from tropical and temperate climate. Quat. Sci. Rev. 30, 2732–2744. doi:10.1016/j.quascirev.2011.06.002

Barrón, V., and Torrent, J. 2002. Evidence for a simple pathway to maghemite in Earth and Mars soils. Geochimica et Cosmochimica Acta 66, 2801–2806, doi:10 .1016 /S0016-7037 (02)00876 -1.

Barrón, V., Torrent, J., de Grave, E 2003. Hydromaghemite, an intermediate in the hydrothermal transformation of 2 line ferrihydrite into hematite. The American Mineralogist 88, 1679–1688, doi:10 .2138 /am -2003 -11 -1207.

Baumgart, P., Hambach, U., Meszner, S., Faust, D. 2013. An environmental magnetic fingerprint of periglacial loess: Records of Late Pleistocene loess-palaeosol sequences from Eastern Germany. Quaternary International 296, 82-93. doi:10.1016/j.quaint.2012.12.021

Begét, J.E., Hawkins, D. B. 1989. Influence of orbital parameters on Pleistocene loess deposits in central Alaska. Nature 337, 151-153. doi:10.1038/337151a0

Benkó, Zs., Molnár, F., Lespinasse, M., Billström, K., Pécskay, Z., Németh, T. 2014.

Triassic fluid mobilization and epigenetic lead-zinc sulphide mineralization in the Transdanubian Shear Zone (Pannonian Basin, Hungary). Geologica Carpathica 65/3, 177-194. DOI: doi:10.2478/geoca-2014-0012

Bidegain, J.C., Evans, M.E., van Velzen, A.J. 2005. A magnetoclimatological investigation of Pampean loess, Argentina. Geophys. J. Int. 160, 55-62. doi:10.1111/j.1365-246X.2004.02431.x

Bidegain, J.C., Rico, Y., Bartel, A., Chaparro, M.A.E., Jurado, s. 2009. Magnetic parameters reflecting pedogenesis in Pleistocene loess deposits of Argentina. Quaternary International 209, 175–186 doi:10.1016/j.quaint.2009.06.024

Boyle, J., F., Dearing, J., A., Blundell, A., Hannam, J., A. 2010. Testing competing hypotheses for soil magnetic susceptibility using a new chemical kinetic model. Geology 38 (12), 1059-1062. doi:10.1130/G31514.1

Buggle, B., Hambach, U., Müller, K., Zöller, L., Marković, S. B., Glaser, B. 2014. Iron mineralogical proxies and Quaternary climate change in SE-European loess–paleosol sequences. Catena 117, 4–22. doi:10.1016/j.catena.2013.06.012

Bradák, B., Újvári, G., Seto, Y., Hyodo, M., Végh, T. 2018a. A conceptual magnetic fabric development model for the Paks loess in Hungary. Aeolian Research 30, 20–31. doi:10.1016/j.aeolia.2017.11.002

Bradák, B., Seto, Y., Hyodo, M., Szeberényi, J. 2018b. Relevance of ultrafine grains in the magnetic fabric of paleosols. Geoderma 330, 125–135.

Bradák, B., Seto, Y., Csonka, D., Végh, T., Szeberényi, J. 2019a. The hematite-goethite enhancement model of loess and an 'irregular' case from Paks, Hungary. Journal of Quaternary Science 1-10. ISSN 0267-8179. DOI: 10.1002/jqs.3101.

Bradák, B., Seto, Y., Nawrocki, J. 2019b. Significant pedogenic and palaeoenvironmental changes during the early Middle Pleistocene in Central Europe. Palaeogeography, Palaeoclimatology, Palaeoecology 534, 109335. doi:10.1016/j.palaeo.2019.109335

Cheng, L., Song, Y., Sun, H., Bradák, B., Orozbaev, R., Zong, X., Liu, H. 2019. Pronounced changes in paleo-wind direction and dust sources during MIS3b recorded in the Tacheng loess, northwest China. Quaternary International. doi:10.1016/j.quaint.2019.05.002 (in press)

Chlachula, J., Evans, M.E., Rutter, N.W. 1998. A magnetic investigation of a Late Quaternary loess/paleosol record in Siberia. Geophys. J. Int. 132, 128-132. doi:10.1046/j.1365-246x.1998.00399.x

Day, R. 1975. Some curious thermomagnetic curves and their interpretation. Earth and Planetary Science Letters 27, 95-100. doi:10.1016/0012-821X(75)90166-1

Day, R., Fuller, M., and Schmidt V. A. 1977. Hysteresis properties of titanomagnetites: Grain size and composition dependence. Phys. Earth Planet. Inter. 13, 260-267. doi:10.1016/0031-9201(77)90108-X

Dearing, J. A., Dann, R. J. L., Hay, K., Lees, J. A., Loveland, P. J., Maher, B. A., O'Grady, K., 1996. Frequency-dependent susceptibility measurements of environmental materials, Geophys. J. Int., 124, 228–240. doi:10.1111/j.1365-246X.1996.tb06366.x

Deng, C., Zhu, R., Verosub, K., Singer, M., Yuan, B. 2000. Paleoclimatic significance of the temperature-dependent susceptibility of Holocene loess along a NW-SE transect in the Chinese Loess Plateau. Geophysical Research Letters, 27(22), 3715–3718. doi:10.1029/2000GL008482

Deng, C., Zhu, R., Jackson, M., Verosub, K., Singer, M. 2001. Variability of the temperature-dependent susceptibility of the Holocene eolian deposits in the Chinese Loess Plateau: A pedogenesis indicator. Physics and Chemistry of the Earth, Part A: Solid Earth and Geodesy, 26(11-12), 873–878. doi:10.1016/S1464-1895(01)00135-1

Dumas, R.K., Li, C-P., Roshchin, I.V., Schuller, I.K., Liu, K. 2007. Magnetic fingerprints of sub-100 nm Fe dots, Physical Review B 75, 134405. doi:10.1103/PhysRevB.75.134405

Dunlop, D. J., 1981. The rock magnetism of fine particles. Phys. Earth Planet. Inter. 26, 1-26. doi:10.1016/0031-9201(81)90093-5

Dunlop D. J. 2002. Theory and application of the Day plot (Mrs/Ms versus Hcr/Hc) 2. Application to data for rocks, sediments, and soils. J. Geophys. Res. 107:No. B3, 2057, 10.1029/2001JB000487, 2002

Dunlop, D. J., Özdemir, Ö., 1997. Rock Magnetism. Fundamentals and Frontiers, Cambridge Studies in Magnetism Series. Cambridge University Press, Cambridge, New York, Port Chester, Melbourne, Sydney 573 p.

Dunlop, D. J., Özdemir, Ö., Rancourt, D. G., 2006. Magnetism of biotite crystals. Earth and Planetary Science Letters, 243. 805–819. doi:10.1016/j.epsl.2006.01.048

Evans, M. E., 2001, Magnetoclimatology of aeolian sediments, Geophys. J. Int., 144, 495-497. doi:10.1046/j.0956-540X.2000.01317.x

Evans, M.E., Heller, F. 1994. Magnetic enhancement and palaeoclimate: study of a loess/palaeosol couplet across the Loess Plateau of China. Geophys. J. Int. 117, 257-264. doi:10.1111/j.1365-246X.1994.tb03316.x

Forster, T., Evans, M.E. & Heller, F., 1994. The frequency dependence of low field susceptibility in loess sediments. Geophys. J. Int., 118, 636–642. doi:10.1111/j.1365-246X.1994.tb03990.x

Fukuma, K., and M. Torii, 1998. Variable shape of magnetic hysteresis loops in the Chinese loess-paleosol sequences. Earth Planets Space 50, 9-14. doi:10.1186/BF03352081

Gao, X., Hao, Q., Oldfield, F., Bloemendal, J., Deng, C., Wang, L., Song, Y., Ge, J., Wu, H., Xu, B., Li, F., Han, L., Fu, Y., Guo, Z. 2019. New high-temperature dependence of magnetic susceptibility-based climofunction for quantifying paleoprecipitation from Chinese loess. Geochemistry, Geophysics, Geosystems, 20, 4273–4291. doi:10.1029/2019GC008401

Geiss, C.E., Zanner, C.W., 2007. Sediment magnetic signature of climate in modern loessic soils from the Great Plains. Quat. Int. 162–163, 97–110. doi:10.1016/j.quaint.2006.10.035

Geiss, C.E., Egli, R., Zanner, C.W., 2008. Direct estimates of pedogenic magnetite as a tool to reconstruct past climates from buried soils. J. Geophys. Res. Solid Earth 113, 1–15. doi:10.1029/2008JB005669

Gocke, M., Hambach, U., Eckmeier, E., Schwark, L., Zöller, L., Fuchs, M., Löscher, M., Wiesenberg, G.L.B., 2014. Introducing an improved multi-proxy approach for paleoenvironmental reconstruction of loess–paleosol archives applied on the late Pleistocene Nussloch sequence (SW Germany). Palaeogeogr. Palaeoclimatol.

Palaeoecol. 410, 300–315. doi:10.1016/j.palaeo.2014.06.006.

Heller, F., Shen, C.D., Beer, J., Liu, X., M., Liu, T.S., Bronger, A, Suter, M., Bonani, G., 1993. Quantitative estimates and palaeoclimatic implications of pedogenic ferromagnetic mineral formation in Chinese loess. Earth Planet. Sci. Letters 114, 385–390. doi:10.1016/0012-821X(93)90038-B

Hrouda, F., 2011. Models of frequency-dependent susceptibility of rocks and soils revisited and broadened, Geophys. J. Int., 187, 1259–1269. doi:10.1111/j.1365-246X.2011.05227.x

Hrouda, F., Jelinek, V., 1990. Resolution of ferromagnetic and paramagnetic anisotropies in rock, using combined low-field and high-field measurements. Geophys. J. Int. 103, 75–84. doi.10.1111/j.1365-246X.1990.tb01753.x

Hu, P., Liu, Q., Torrent, J., Barrón, V., Jin, C. 2013. Characterizing and quantifying iron oxides in Chinese loess/paleosols: Implications for pedogenesis. Earth and Planetary Science Letters 369–370, 271–283. doi:10.1016/j.epsl.2013.03.033

Hu, P., Liu, Q., Heslop, D., Roberts, A.P., Jin, C., 2015. Soil moisture balance and magnetic enhancement in loess–paleosol sequences from the Tibetan Plateau and Chinese Loess Plateau. Earth and Planetary Science Letters 409, 120-132. doi:10.1016/j.epsl.2014.10.035

Hyodo, M., Sano, T., Matsumoto, M., Seto, Y., Bradák, B., Suzuki, K., Fukuda, J-i., Shi, M., Yang, T. 2020. Nanosized authigenic magnetite and hematite particles in mature-paleosol phyllosilicates: New evidence for a magnetic enhancement mechanism in loess sequences of China. Journal of Geophysical Research: Solid Earth, 125, e2019JB018705. doi:10.1029/2019JB018705

Ji, J.F., Balsam, W., Chen, J., 2001. Mineralogic and climatic interpretations of the Luochuan loess section (China) based on diffuse reflectance spectrophotometry. Quaternary Research 56, 23–30. doi:10.1006/qres.2001.2238

Ji, J.F., Balsam, W., Chen, J., Liu, L.W., 2002. Rapid and quantitative measurement of hematite and goethite in the Chinese loess–paleosol sequence by diffuse reflectance spectroscopy. Clays and Clay minerals 50, 208–216. doi:10.1346/000986002761832801

Ji, J.F., Chen, J., Balsam, W., Lu, H., Sun, Y., Xu, H., 2004. High resolution hematite/goethite records from Chinese loess sequences for the last glacial–interglacial cycle: Rapid climatic response of the East Asian Monsoon to the tropical Pacific. Geophysical Research Letters 31, L03207. doi:10.1029/2003GL018975.

Jiang, Z., Liu, Q., Colombo, C., Barrón, V., Torrent, J., Hu, P., 2013. Quantification of Al-goethite from diffuse reflectance spectroscopy and magnetic methods, Geophys. J.

Int. Geomagnetism, rock magnetism and palaeomagnetism, 1-14. doi:10.1093/gji/ggt377

Jiang, Z., Liu, Q., Roberts, A.P., Barrón, V., Torrent, J., Zhang, Q., 2018. A new model for transformation of ferrihydrite to hematite in soils and sediments. Geology 46, 1-4. doi:10.1130/G45386.1.

Jin, C., Liu, Q. 2010. Reliability of the natural remanent magnetization recorded in Chinese loess. Journal of Geophysical Research 115: B04103, doi:10.1029/2009JB006703.

Költringer, C.A., Stevens, T., Almqvist, B., Bradák, B., Kurbanov, R., Snowball, I., Yarovaya, S. 2020. Mineral magnetic record of Late Quaternary environmental evolution in Lower Volga loess sequences, Russia. Quaternary Research (under review), QUA-20-1

Kravchinsky, V.A., Zykina, V.S., Zykin, V.S. 2008. Magnetic indicator of global paleoclimate cycles in Siberian loess–paleosol sequences. Earth and Planetary Science Letters 265, 498-514. doi:10.1016/j.epsl.2007.10.031

Lagroix, F., Banerjee, S. K., 2002.Paleowind direction from the magnetic fabric of loess profile in central Alaska. Earth and Planetary Science Letters 195, 99-102. doi:10.1016/S0012-821X(01)00564-7

Leonhardt, R. 2006. Analyzing rock magnetic measurements: The RockMagAnalyzer 1.0 software. Computers & Geosciences 32, 1420-1431. doi:10.1016/j.cageo.2006.01.006

Li, G., Xia, D., Appel, E., Wang, Y., Jia, J., Yang, X. 2018. A paleomagnetic record in loess–paleosol sequences since late Pleistocene in the arid Central Asia. Earth, Planets and Space 70:44. doi:10.1186/s40623-018-0814-8

Liu, Q.S., Barrón, V., Torrent, J., Eeckhout, S., Deng, C. 2008. Magnetism of intermediate hydromaghemite in the transformation of 2-line ferrihydrite into hematite and its paleoenvironmental implications: Journal of Geophysical Research 113, B01103, doi:10.01029/02007JB005207.

Liu, Q., Torrent, J., Barrón, V., Duan, Z. Q., Bloemendal, J. 2011. Quantification of hematite from the visible diffuse reflectance spectrum: effects of aluminium substitution and grain morphology. Clay Minerals 46, 137–147. doi:10.1180/claymin.2011.046.1.137

Liu, X., Shaw, J., Liu, T., Heller, F., Yuan, B. 1992. Magnetic mineralogy of Chinese loess and its significance. Geophys. J. Int. 108, 301-308. doi:10.1111/j.1365-246X.1992.tb00859.x

Liu, X.M., Shaw, J., Jiang, J.Z., Bloemendal, J., Hesse, P., Rolph, T., Mao, X.G., 2010.

Analysis on variety and characteristics of maghemite, Sci. China Earth Sci., 53, 1–6.

Liu, Y., Shi, Z., Deng, C., Su, H., Zhang, W. 2012. Mineral magnetic investigation of the Talede loess–palaeosol sequence since the last interglacial in the Yili Basin in the Asian interior. Geophys. J. Int.190, 267–277 doi: 10.1111/j.1365-246X.2012.05527.x

Liu, Z., Liu, Q., Torrent, J., Barrón, V., Hu, P. 2013. Testing the magnetic proxy χFD/HIRM for quantifying paleoprecipitation in modern soil profiles from Shaanxi Province, China, Glob. Planet. Change, 110, 368–378. doi:10.1016/j.gloplacha.2013.04.013

Long, X., Ji, J., Barr, V., 2016. Climatic thresholds for pedogenic iron oxides under aerobic conditions : Processes and their significance in paleoclimate reconstruction. Quat. Sci. Rev. 150, 264–277. doi:10.1016/j.quascirev.2016.08.031

Ma, M., Liu, X., Hesse, P.P., Lü, B., Guo, X., Chen, J. 2013. Magnetic properties of loess deposits in Australia and their environmental significance. Quaternary International 296, 198-205. doi:10.1016/j.quaint.2012.06.018

Maher, B. A. 2011. The magnetic properties of Quaternary aeolian dusts and sediments, and their palaeoclimatic significance. Aeolian Research 3, 87–144. doi:10.1016/j.aeolia.2011.01.005

Maher, B. A. 2016. Palaeoclimatic records of the loess/palaeosol sequences of the

Chinese Loess Plateau. Quaternary Science Reviews 154, 23-84. doi:10.1016/j.quascirev.2016.08.004

Maher, B.A., Taylor, R.M., 1988. Formation of ultrafine-grained magnetite in soils, Nature, 336, 368–370. doi:10.1038/336368a0

Maher, B.A., Alekseev, A., Alekseeva, T., 2002. Variation of soil magnetism across the Russian steppe: Its significance for use of soil magnetism as a palaeorainfall proxy. Quat. Sci. Rev. 21, 1571–1576. doi:10.1016/S0277-3791(02)00022-7

Maher, B.A., Alekseev, A., Alekseeva, T., 2003. Magnetic mineralogy of soils across the Russian Steppe: Climatic dependence of pedogenic magnetite formation. Palaeogeogr. Palaeoclimatol. Palaeoecol. 201, 321–341. doi:10.1016/S0031-0182(03)00618-7

Maher, B.A., Thompson, R., Zhou, L.P., 1994. Spatial and temporal reconstructions of changes in the Asian palaeomonsoon: A new mineral magnetic approach. Earth Planet. Sci. Lett. 125, 461–471. doi:10.1016/0012-821X(94)90232-1

Makvandi, S., Beaudoi, G., McClenaghan, B.M., Layton-Matthews, D. 2015. The surface texture and morphology of magnetite from the Izok Lake volcanogenic massive sulfide deposit and local glacial sediments, Nunavut, Canada: Application to mineral exploration. Journal of Geochemical Exploration 150, 84–103

Marković S. B., Hambach, U., Stevens T., Kukla, G.J., Heller, F., McCoy, W.D., Oches, E.A., Buggle, B., Zöller, L. 2011. The last million years recorded at the Stari Slankamen (Northern Serbia) loess-palaeosol sequence: revised chronostratigraphy and long-term environmental trends. Quaternary Science Reviews 30, 1142–1154. doi:10.1016/j.quascirev.2011.02.004

Marković SB, Stevens T, Kukla GJ, Hambach U, Fitzsimmons KE, Gibbard P, Buggle B, Zech M, Guo Z, Hao Q, Wu H, O'Hara Dhand K, Smalley I, Újvári G, Sümegi P, Timar-Gabor A, Veres D, Sirocko F, Vasiljević DA, Jary Z, Svensson A, Jović V, Lehmkuhl F, Kovács J, Svirčev Z. 2015. Danube loess stratigraphy — Towards a pan-European loess stratigraphic model. Earth-Science Reviews 148, 228-258. doi:10.1016/j.earscirev.2015.06.005

Mush, D.R. 2007. Loess deposit, origins and properties. In: Elias, S.A. (ed.) Encyclopedia of Quaternary Science, ELSEVIER, pp. 1405-1418.

Nadoll, P., Angerer, T., Mauk, J.L., French, D., Walshe, J. 2014. The chemistry of hydrothermal magnetite: A review. Ore Geology Reviews 61, 1-32. doi:10.1016/j.oregeorev.2013.12.013

Necula, C., Dimofte, D., Panaiotu, C. 2015. Rock magnetism of a loess-palaeosol sequence from the western Black Sea shore (Romania). Geophys. J. Int. 202, 1733–

1748 doi: 10.1093/gji/ggv250

Obreht, I., Zeeden, C., Hambach, U., Veres, D., Marković, S.B., Bösken, J., Svirčev, Z., Bačević, N., Gavrilov, M.B., Lehmkuhl, F., 2016. Tracing the influence of Mediterranean climate on Southeast Europe during the past 350,000 years. Scientific Reports 6, 36334.DOI:10.1038/srep36334

Orgeira, M.J., Egli, R., Compagnucci, R.H., 2011. A quantitative model of magnetic enhancement in loessic soils, in: Petrovský, E., Ivers, D., Harinarayana, T., Herrero-Bervera, E. (Eds.), The Earth's Magnetic Interior. IAGA Special Sopron Book Series book series (IAGA, volume 1), pp. 361-397. doi:10.1007/978-94-007-0323-0

Pan, Y., Zhu, R., Liu, Q., Gus B., Yue, L., Wu, H. 2002. Geomagnetic episodes of the last 1.2 Myr recorded in Chinese loess. Geophysical Research Letters 29, 1282, doi:10.1029/2001GL014024

Panaiotu, C.G., Panaiotu, E.C., Grama, A., Necula, C., 2001. Paleoclimatic record from a loess-paleosol profile in Southeastern Romania. Phys. Chem. Earth, Part A Solid Earth Geod. 26, 893–898. doi:10.1016/S1464-1895(01)00138-7

Pye, K. 1987. Aeolian dust and dust deposits. Academic Press, San Diego, CA, 330p.

Richter, C., van der Pluijm, B. A. 1994. Separation of paramagnetic and ferrimagnetic

susceptibilities using low temperature magnetic susceptibilities and comparison with high field methods. Physics of the Earth and Planetary Interiors 82, 113-123. doi:10.1016/0031-9201(94)90084-1

Roberts, A.P., Pike, C.R., Verosub K.L. 2000. First-order reversal curve diagrams: A new tool for characterizing the magnetic properties of natural samples. J. Geophys. Res. 105:28,461-28,465.

Rochette, P., 1987. Magnetic susceptibility of the rock matrix related to the magnetic fabric studies. J. Struct. Geol. 9, 1015–1020. doi:10.1016/0191-8141(87)90009-5

Roberts, A. P., Almeida, T. P., Church, N. S., Harrison, R. J., Heslop, D., Li, Y., Li, J., Muxworthy, A. R., Williams, W., Zhao, X. 2017. Resolving the origin of pseudo-single domain magnetic behaviour. Journal of Geophysical Research: Solid Earth 122:9534–9558. doi:10.1002/2017JB014860

Sano, T., Hyodo, M., Matsumoto, M. & Seto, Y., 2017. Exploration of pedogenic nanoscale particles causing magnetic enhancement in Chinese loess deposits, SEM20-13, Japan Geoscience Union, JpGU-AGU Joint Meeting 20th – 25th of May, Makuhari Messe, Chiba, Japan, 2017. https://confit.atlas.jp/guide/event-img/jpguagu2017/SEM20-13/public/pdf?type=in

Schaetzl, R. J., Bettis, E. A., Crouvi, O., Fitzsimmons, K. E., Grimley, D. A., Hambach,

U., Lehmkuhl, F., Marković, S. B., Mason, J. A., Owczarek, P., Roberts, H. M., (a12), Rousseau, D-D., Stevens, T., Vandenberghe, J., Zárate, M., Veres, D., Yang, S., Zech, M., Conroy, J. L., Dave, A. K., Faust, D., Hao, Q., Obreht, I., Prud'homme, C., Smalley, I., Tripaldi, A., Zeeden, C., Zech, R. 2018. Approaches and challenges to the study of loess—Introduction to the LoessFest Special Issue, Quaternary Research 89 (3), 563-618. doi:10.1017/qua.2018.15

Schellenberger, A., Heller, F., Veit, H. 2003. Magnetostratigraphy and magnetic susceptibility of the Las Carreras loess–paleosol sequence in Valle de Tafí, Tucumán, NW-Argentina. Quaternary International 106–107, 159–167. doi:10.1016/S1040-6182(02)00170-2

Spassov, S., Heller, F., Kretzschmar, R., Evans, M.E., Yue, L.P., Nourgaliev, D.K. 2003. Detrital and pedogenic magnetic mineral phases in the loess/palaeosol sequence at Lingtai (Central Chinese Loess Plateau). Physics of the Earth and Planetary Interiors 140, 255–275. doi:10.1016/j.pepi.2003.09.003

Stevens, T., Sechi, D., Bradák, B., Orbe, R., Cossu, G., Tziavaras, C., Baykal, Y., Andreucci, S., Pascucci, V. 2020. Abrupt last glacial dust fall over Southeast England associated with dynamics of the British-Irish Ice Sheet. Quaternary Science Reviews 250, 106641, doi:10.1016/j.quascirev.2020.106641

Taylor, S.N., Lagroix, F., Rousseau, D.-D., Antoine, P., 2014. Mineral magnetic characterization of the Upper Pleniglacial Nussloch loess sequence (Germany): an insight into local environmental processes. Geophys. J. Int. 199:1463–1480. doi: 10.1093/gji/ggu331

Torrent J, Liu Q, Bloemendal J, Barrón V. 2007. Magnetic Enhancement and Iron Oxides in the Upper Luochuan Loess–Paleosol Sequence, Chinese Loess Plateau. Soil Sci. Soc. Am. J. 71 : 1570–1578 doi:10.2136/sssaj2006.0328

Toucanne, S., Zaragosi, S., Bourillet, J. F., Gibbard, P.L. Eynaud, F., Giraudeau, J., Turon, J. L., Cremer, M., Cortijo, F., Martinez, P., and Rossignol, L., 2009, A 1.2 Ma record of glaciation and fluvial discharge from the West European Atlantic margin: Quaternary Science Reviews 28, 2974-2981.

Újvári, G., Varga, A., Ramos, F. C., Kovács, J., Németh, T., Stevens, T., 2012. Evaluating the use of clay mineralogy, Sr–Nd isotopes and zircon U–Pb ages in tracking dust provenance: An example from loess of the Carpathian Basin. Chemical Geology, 304–305, 83–96. doi:10.1016/j.chemgeo.2012.02.007

Újvári G, Varga A, Raucsik B, Kovács J. 2014. The Paks loess-paleosol sequence: a record of chemical weathering and provenance for the last 800 ka in the mid-Carpathian Basin. Quaternary International 319, 22-37.

doi:10.1016/j.quaint.2012.04.004

Újvári, G., Kok, J.F., Varga, G., Kovács, J., 2016. The physics of wind-blown loess: implications for grain size proxy interpretations in Quaternary paleoclimate studies. Earth-Science Reviews 154, 247–278.

Thamó-Bozsó, E., Kovács, L. Ó., Magyari, Á. & Marsi I., 2014. Tracing the origin of loess in Hungary with the help of heavy mineral composition data, Quaternary International, 319, 11–21. doi:10.1016/j.quaint.2013.04.030

Yang, T., Hyodo, M., Zhang, S., Maeda, Yang, L. Wu, H. & Li, H., 2013. New insights into magnetic enhancement mechanism in Chinese paleosols, Palaeogeography, Palaeoclimatology, Palaeoecology, 369, 493–500. doi:10.1016/j.palaeo.2012.11.016

van Velzen, A.J., Dekkers, M.J., 1999. Low-temperature oxidation of magnetite in loess-paleosol sequences: a correction of rock magnetic parameters. Studia geophysica et geodaetica 43 (4), 357-375. doi:10.1023/A:1023278901491

Vos, K., Vandenberghe, N., Elsen, J. 2014. Surface textural analysis of quartz grains by scanning electron microscopy (SEM): From sample preparation to environmental interpretation. Earth-Science Reviews 128, 93–104. doi:10.1016/j.earscirev.2013.10.013

Wacha, L., Rolf, C., Hambach, U., Frechen, M., Galović, L., Duchoslav, M. 2018. The

Last Glacial aeolian record of the Island of Susak (Croatia) as seen from a high-resolution grain-size and rock magnetic analysis. Quaternary International 494, 211-224. doi:10.1016/j.quaint.2017.08.016

Wang, X., Lu, H., Xu, H., Deng, C., Chen, T., Wang, Xi. 2006. Magnetic properties of loess deposits on the northeastern Qinghai-Tibetan Plateau: palaeoclimatic implicationsfor the Late Pleistocene. Geophys. J. Int. 167, 1138-1147, doi: 10.1111/j.1365-246X.2006.03007.x

Zeeden, C., Kels, H., Hambach, U., Schulte, P., Protze, J., Eckmeier, E., Marković, S.B., Klasen, N., Lehmkuhl, F. 2016. Three climatic cycles recorded in a loess-palaeosol sequence at Semlac (Romania) – implications for dust accumulation in south-eastern Europe. Quaternary Science Reviews 154, 130-142. doi:10.1016/j.quascirev.2016.11.002

Zeeden, C., Hambach, U., Veres, D., Fitzsimmons, K., Obreht, I., Bösken, J., Lehmkuhl, F. 2018. Millennial scale climate oscillations recorded in the Lower Danube loess over the last glacial period. Palaeogeography, Palaeoclimatology, Palaeoecology 509, 164-181. doi:10.1016/j.palaeo.2016.12.029

Zhou, L.P., Oldfield, F., Wintle, A.G., Robinson, S.G., Wang, T.J. 1990. Partly pedogenic origin of magnetic variations in Chinese loess. Nature 346, 737-739.

doi:10.1038/346737a0

Zhu, R., Deng, C., Jackson, M. J. 2001. A magnetic investigation along a NW-SE transect of the Chinese Loess Plateau and its implications. Physics and Chemistry of the Earth, Part A: Solid Earth and Geodesy, 26(11-12), 867–872. doi:10.1016/S1464-1895(01)00134-X

Supplementary Materials

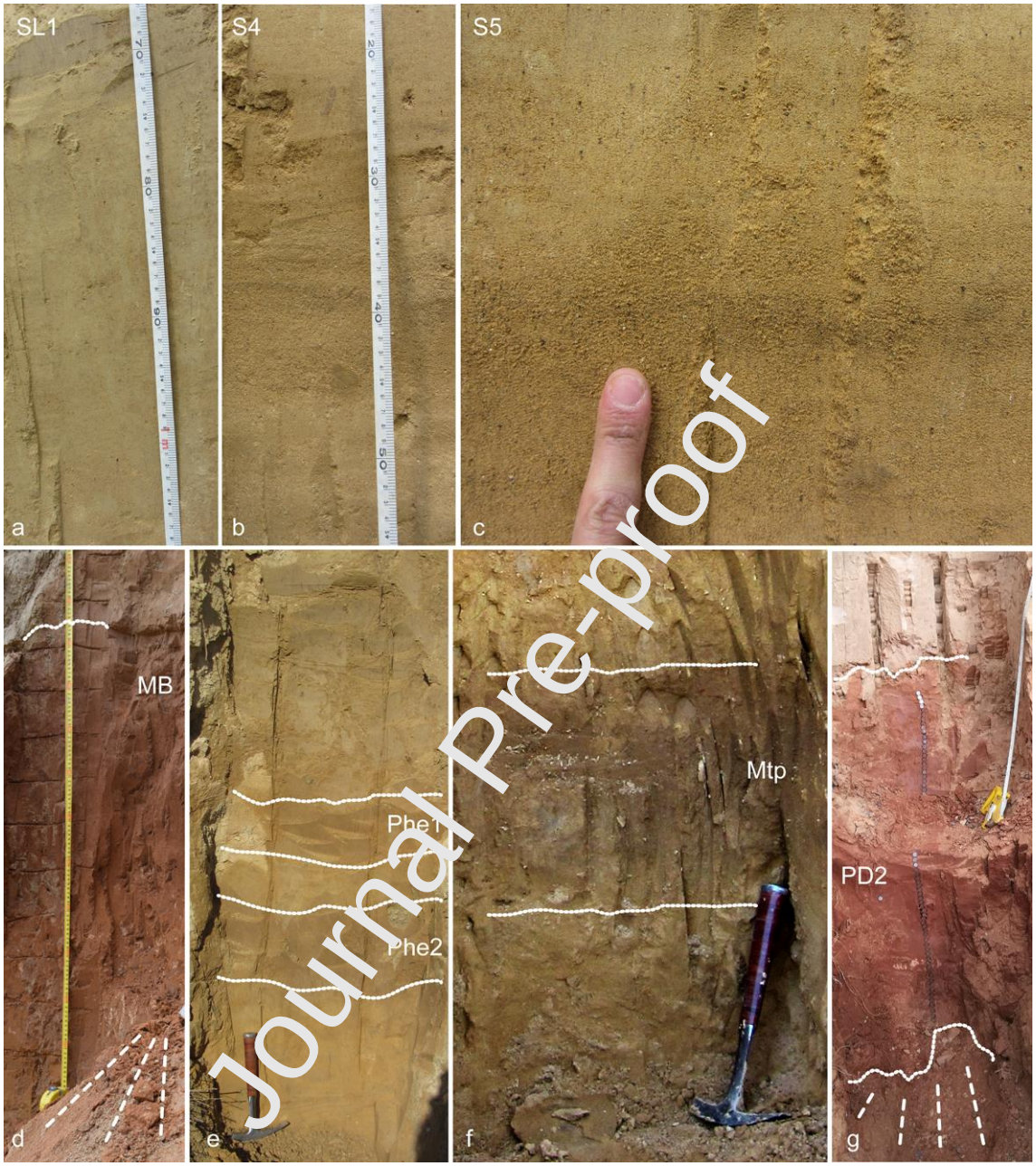

Suppl. Mat. 1. Characteristic units of the studied PK section. a) typical aeolian loess from the SL1 sandy loess unit; b and c) fine sand and silt horizons in the S4-S5 units; d) MB (MIS11) paleosol horizon; e) Phe1 and 2 weakly developed paleosol horizons; f) Mtp paleosol unit (MIS15); and g) PD2 (MIS19) paleosol unit. The dashed lines indicate debris.

Suppl. Mat. 2. The separation of EXT and RESIDf and c extract in the laboratory.

Suppl. Mat. 3. Collection of various loess magnetic data used in the study.

Suppl. Mat. 4. The summary of applied methods, their purpose, the results and their relation in loess research. a) The setting of strong magnets immersed in the silt-sand suspensions; b) the EXT extract on the surface of the plastic tube after 24 hours of rest in the suspension; c) collection of EXT from the surface of the plastic tube; d) EXT, prepared for drying; and e) phyllosilicates in RESIDc.

Profile (ref); [n-number of samples]	Loess region	Equation of magnetic enhancement trend	r, [p(a)<0.05]	Backg. susc. (×10-8 m^3/kg)
Raigorod (RG; Költringer et al. 2020); [216]	East European Plain	y = 39.87x + 4.3659	0.93	4.4
Paks (PK) (4 kHz); [141]	Middle Danube Basin	y = 26.532x + 10.04	0.95	10.0
Paks (PK) (16 kHz); [141]	Middle Danube Basin	y = 44.219x + 10.04	0.95	10.0
Semlac (Se; Zeeden et al., 2016); [215]	Middle Danube Basin	y = 15.346x + 10.294	0.99	10.3
Titel composite section (TI; Marković et al., 2011); [1229]	Middle Danube Basin	y = 16.391x + 10.383	0.99	10.4
Srednaya Akhtuba (SA; Költringer et al., 2020); [103]	East European Plain	y = 19.695x + 12.296	0.56	12.3
Leninsk (LN; Költringer et al., 2020);[315]	East European Plain	y = 8.0712x + 14.882	0.57	14.9
Dunaszekcső (DSZ; Újvári et al., 2016); [315]	Middle Danube Basin	y = 16.944x + 18.561	0.99	18.6
Rasova-Valea cu Pietre (RVP; Zeeden et al., 2018); [348]	Lower Danube Basin	y = 16.67x + 30.333	0.90	30.3
Stalać (ST; Obreht et al., 2016); [410]	Lower Danube Basin	y = 25.111x + 93.001	0.67	93.0

Theories, models	Phenomena	Short description	Loess region	References (e.g.)
Pedogenic enhancement model	increasing χlf, increasing χfd	Magnetic enhancement of loess by in situ authigenic mineral forming during paedogenesis	CLP, ELB,	Heller et al. (1993); Maher et al. (1994, 2002, 2003); Panaiotu et al. (2001); Orgeira et al. (2011)
Wind-vigour model	low χlf in paleosols, high χlf in loess	Increasing input of dense magnetic particles by stronger, more frequent winds during glacial periods	Alaska, Siberia, ELB	Begét and Hawkins (1989); Chachula et al. (1998)
Lithological differences in the source area of the dust (theoretical)	low χlf in paleosols, high χlf in loess	Different source area of dust during glacial and interglacial periods	Pampean loess	Schellenberger et al. (2003)
Combined pedogenic and wind-vigour model	low χlf and high fd in paleosols, high χlf in loess	The combination of the two main theories described above	Central Asia, CLP, ELB, Pampean loess, Siberia	Bidegain et al. (2005); Wang et al. (2006); Kravchinsky et al. (2008); Stevens et al. (2020)
Magnetic mineral dissolution	high χlf, low χfd	Dissolution of mainly fine-grain magnetic contributors by hydromorphic processes	ELB	Taylor et al. (2014)
Magnetic mineral alteration	low χlf, relatively high χfd	The gradual conversion of magnetite and maghemite to goethite in a humid environment (~940 mm/year)	Australian loess/parna	Ma et al. (2013)
Fragmentation by chemical weathering	low χlf, relatively high χfd	Destruction of coarse (detrital sedimentary) magnetic particles by strong weathering in paleosols	ELB	Bidegain et al. (2009); Baumgart et al. (2013); Gocke et al. (2014); Ghafarpour et al. (2016)
Surface oxidation ("detrital magnetic enhancement")	incr. χlf, relatively high χfd	Surface oxidation of coarse magnetic grains, and ultrafine magnetic mineral forming on their surface	ELB	Buggle et al. (2014); Wacha et al. (2018); Zeeden et al. (2018); Stevens et al. (2020)
Nanofragmentation (by physical weathering)	low χlf, relatively high χfd	Fragmentation of coarser sedimentary magnetic particles by physical processes during	ELB	in this study

		transportation and diagenesis		
Lithogenic inherited magnetic enhancement, “lithogenic enh.”	low χlf, relatively high χfd	Inherited fine-grain magnetic inclusions in phyllosilicates from the source rock of the dust	ELB	in this study

- The ways of magnetic enhancement in loess are summarised
- New ways of detrital enhancement of magnetic susceptibility are introduced
- A guide for the interpretation of low field and frequency dependent susceptibility is introduced

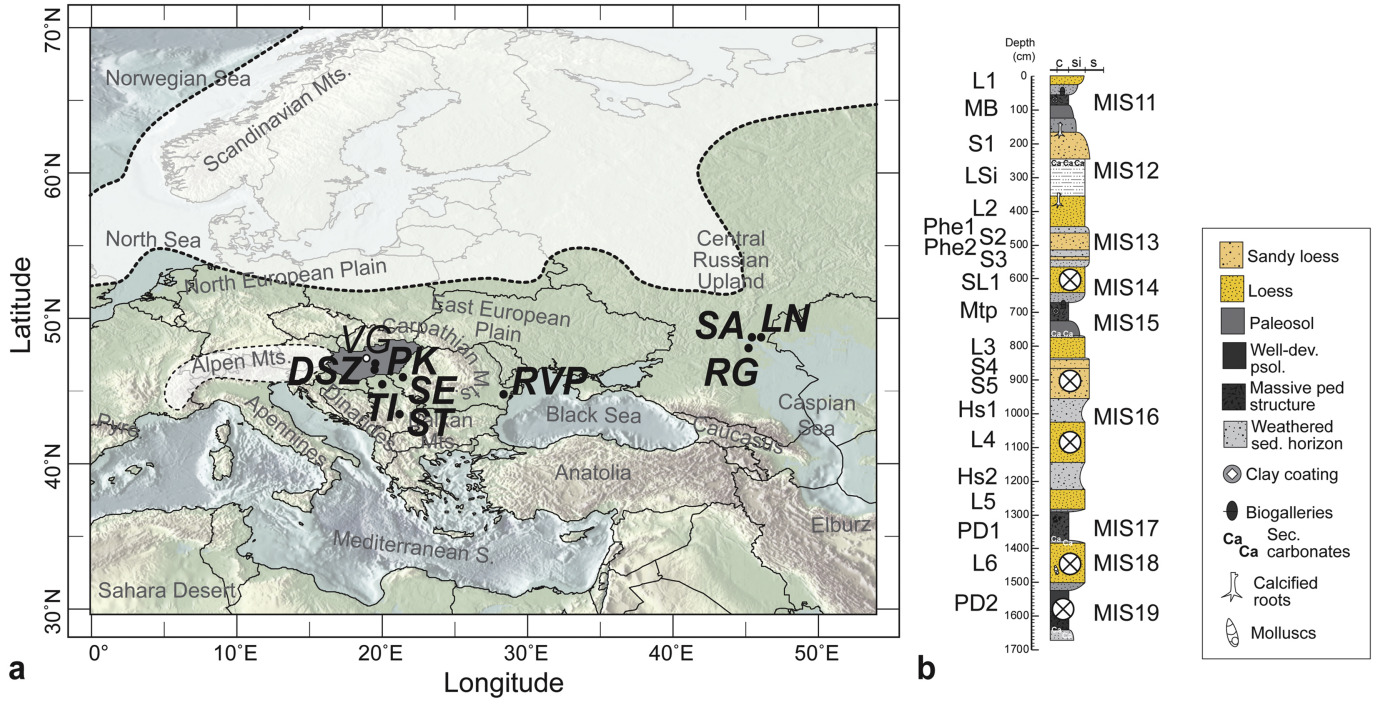
Norwegian Sea
Scandinavian Mts.
North Sea
North European Plain
Central Russian Upland
East European Plain
Carpathian Mts.
Alpen Mts.
Dinarides
Apennines
Pyrs.
Black Sea
Caucasus
Caspian Sea
Anatolia
Elburz
Mediterranean S.
Sahara Desert
VG
PK
DSZ
SE
TI
ST
RVP
SA
LN
RG
70°N
60°N
50°N
40°N
30°N
0°
10°E
20°E
30°E
40°E
50°E
Latitude
Longitude
a
Depth (cm)
c si s
L1
MB
S1
LSi
L2
Phe1
Phe2
S2
S3
SL1
Mtp
L3
S4
S5
Hs1
L4
Hs2
L5
PD1
L6
PD2
MIS11
MIS12
MIS13
MIS14
MIS15
MIS16
MIS17
MIS18
MIS19
Sandy loess
Loess
Paleosol
Well-dev. psol.
Massive ped structure
Weathered sed. horizon
Clay coating
Biogalleries
Sec. carbonates
Calcified roots
Molluscs
b

Figure 1

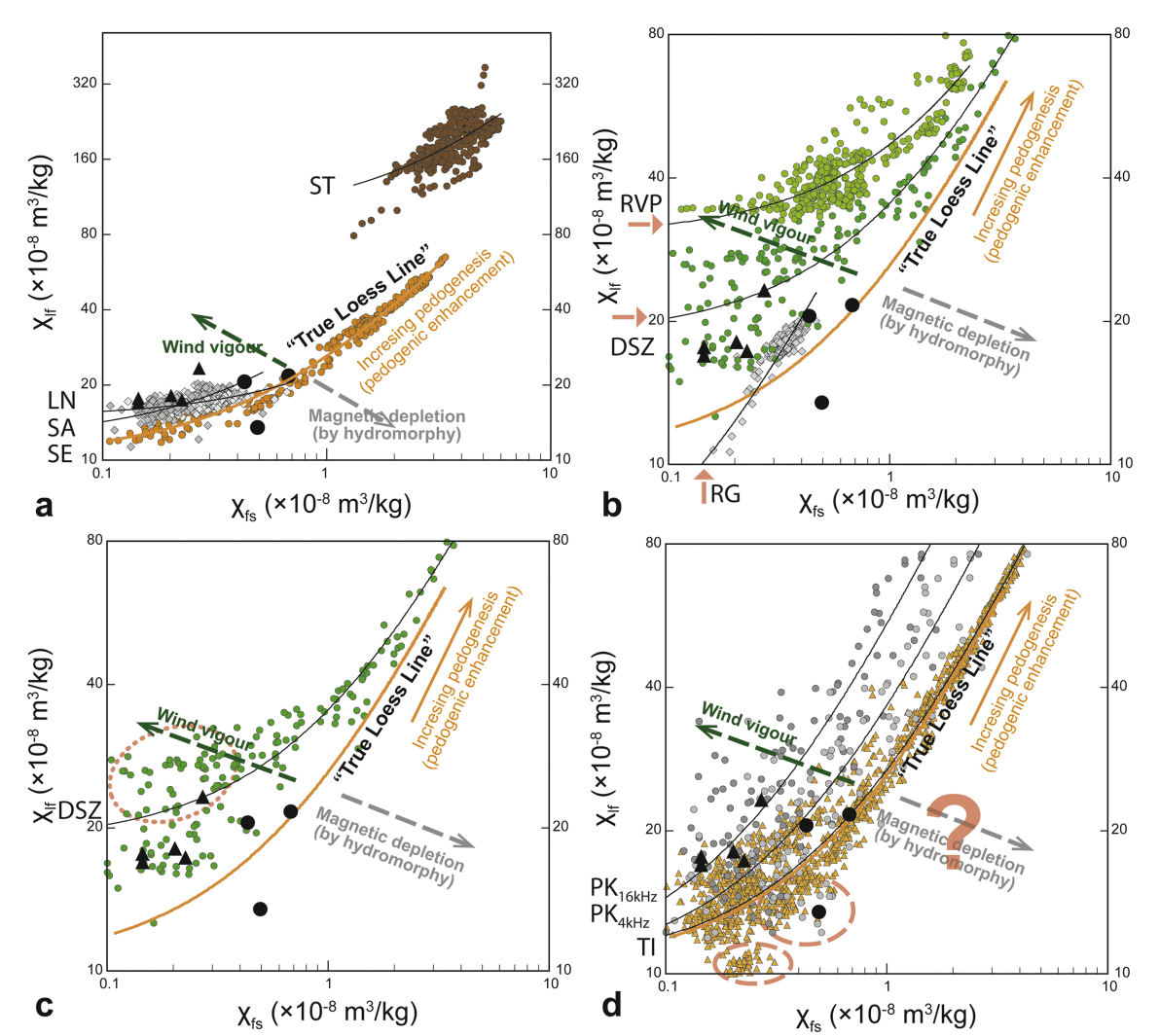
a
b
c
d
ST
LN
SA
SE
RVP
DSZ
RG
TI
PK16kHz
PK4kHz
Wind vigour
"True Loess Line"
Increasing pedogenesis (pedogenic enhancement)
Magnetic depletion (by hydromorphy)
χlf (×10-8 m3/kg)
χfs (×10-8 m3/kg)
DSZ LN PK(4 and 16 kHz) RG RVP SA ST SE TI

Figure 2

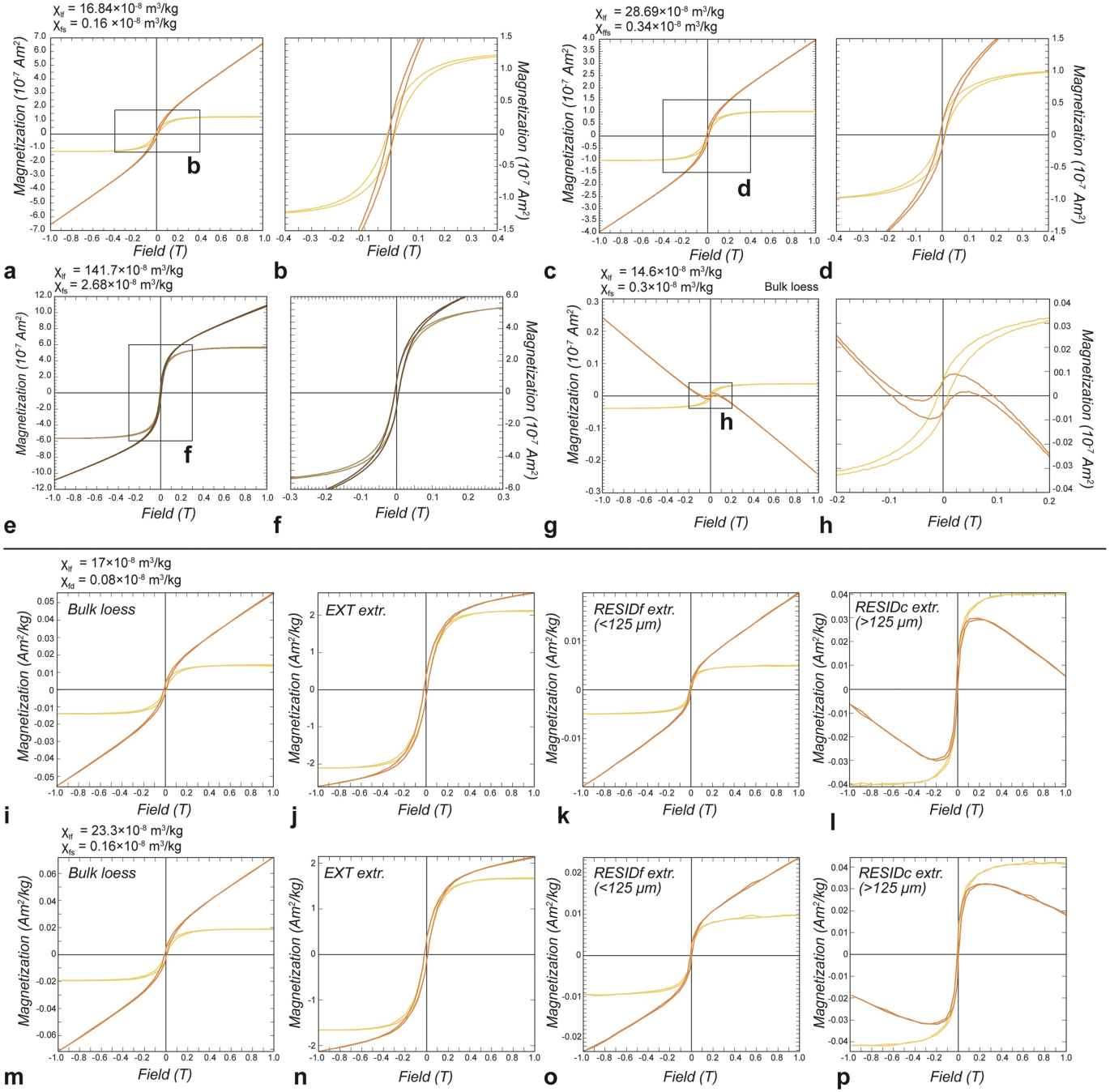
χlf = 16.84×10-8 m3/kg
χfs = 0.16 ×10-8 m3/kg
χlf = 28.69×10-8 m3/kg
χffs = 0.34×10-8 m3/kg
χlf = 141.7×10-8 m3/kg
χfs = 2.68×10-8 m3/kg
χlf = 14.6×10-8 m3/kg
χfs = 0.3×10-8 m3/kg
Bulk loess
χlf = 17×10-8 m3/kg
χfd = 0.08×10-8 m3/kg
Bulk loess
EXT extr.
RESIDf extr. (<125 μm)
RESIDc extr. (>125 μm)
χlf = 23.3×10-8 m3/kg
χfs = 0.16×10-8 m3/kg
Bulk loess
EXT extr.
RESIDf extr. (<125 μm)
RESIDc extr. (>125 μm)
Magnetization (10-7 Am2)
Magnetization (Am2/kg)
Field (T)
a
b
c
d
e
f
g
h
i
j
k
l
m
n
o
p

Figure 3

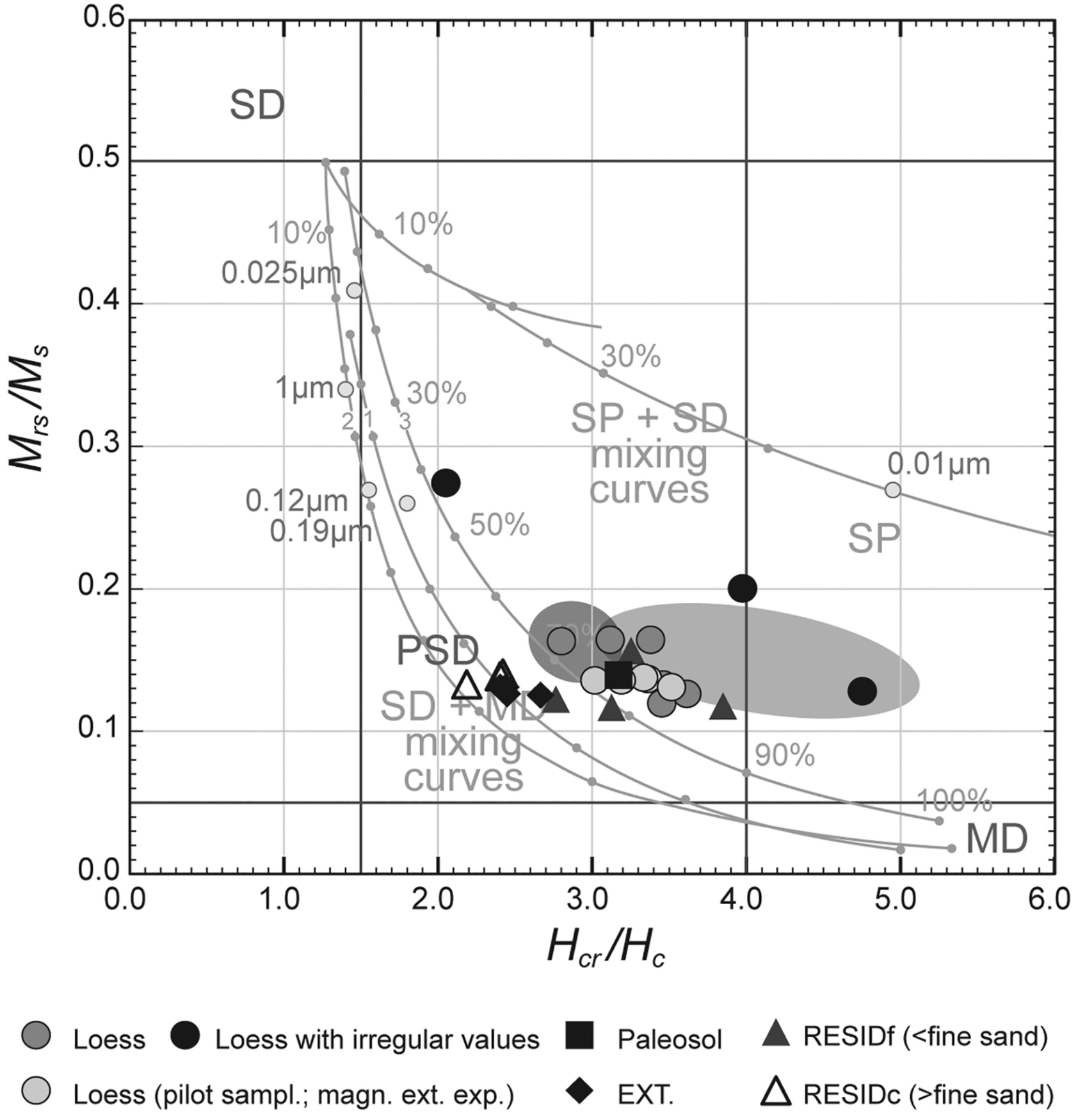
SD
PSD
MD
SP + SD mixing curves
SD + MD mixing curves
SP
10%
30%
50%
70%
90%
100%
0.025µm
1µm
0.12µm
0.19µm
0.01µm
2
1
3
M_{rs}/M_s
H_{cr}/H_c
0.0
0.1
0.2
0.3
0.4
0.5
0.6
1.0
2.0
3.0
4.0
5.0
6.0
Loess
Loess with irregular values
Paleosol
RESIDf (<fine sand)
Loess (pilot sampl.; magn. ext. exp.)
EXT.
RESIDc (>fine sand)

Figure 4

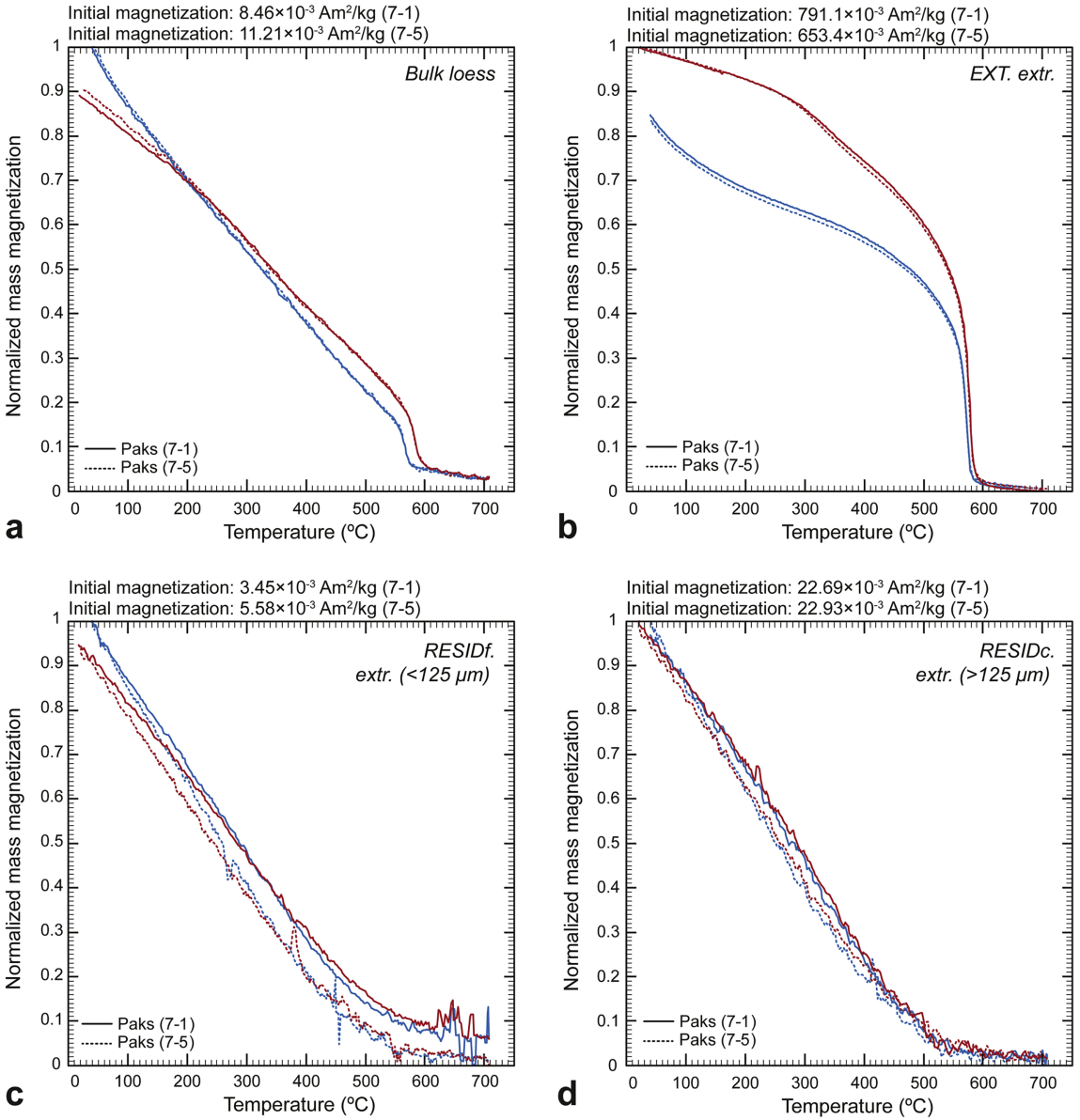
Initial magnetization: 8.46×10-3 Am2/kg (7-1)
Initial magnetization: 11.21×10-3 Am2/kg (7-5)
Bulk loess
Normalized mass magnetization
Paks (7-1)
Paks (7-5)
Temperature (ºC)
a
Initial magnetization: 791.1×10-3 Am2/kg (7-1)
Initial magnetization: 653.4×10-3 Am2/kg (7-5)
EXT. extr.
Normalized mass magnetization
Paks (7-1)
Paks (7-5)
Temperature (ºC)
b
Initial magnetization: 3.45×10-3 Am2/kg (7-1)
Initial magnetization: 5.58×10-3 Am2/kg (7-5)
RESIDf.
extr. (<125 μm)
Normalized mass magnetization
Paks (7-1)
Paks (7-5)
Temperature (ºC)
c
Initial magnetization: 22.69×10-3 Am2/kg (7-1)
Initial magnetization: 22.93×10-3 Am2/kg (7-5)
RESIDc.
extr. (>125 μm)
Normalized mass magnetization
Paks (7-1)
Paks (7-5)
Temperature (ºC)
d

Figure 5

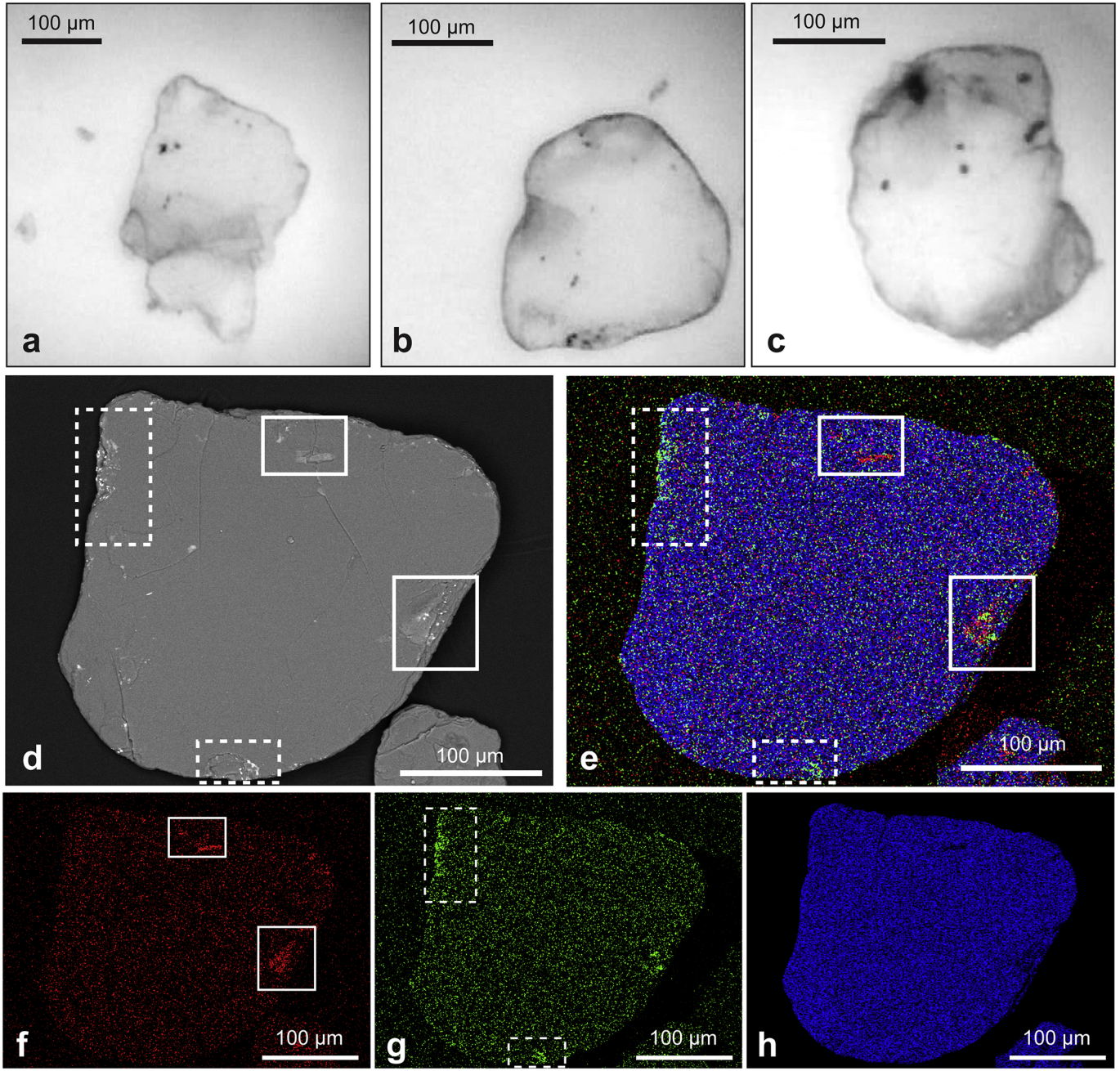

Figure 6

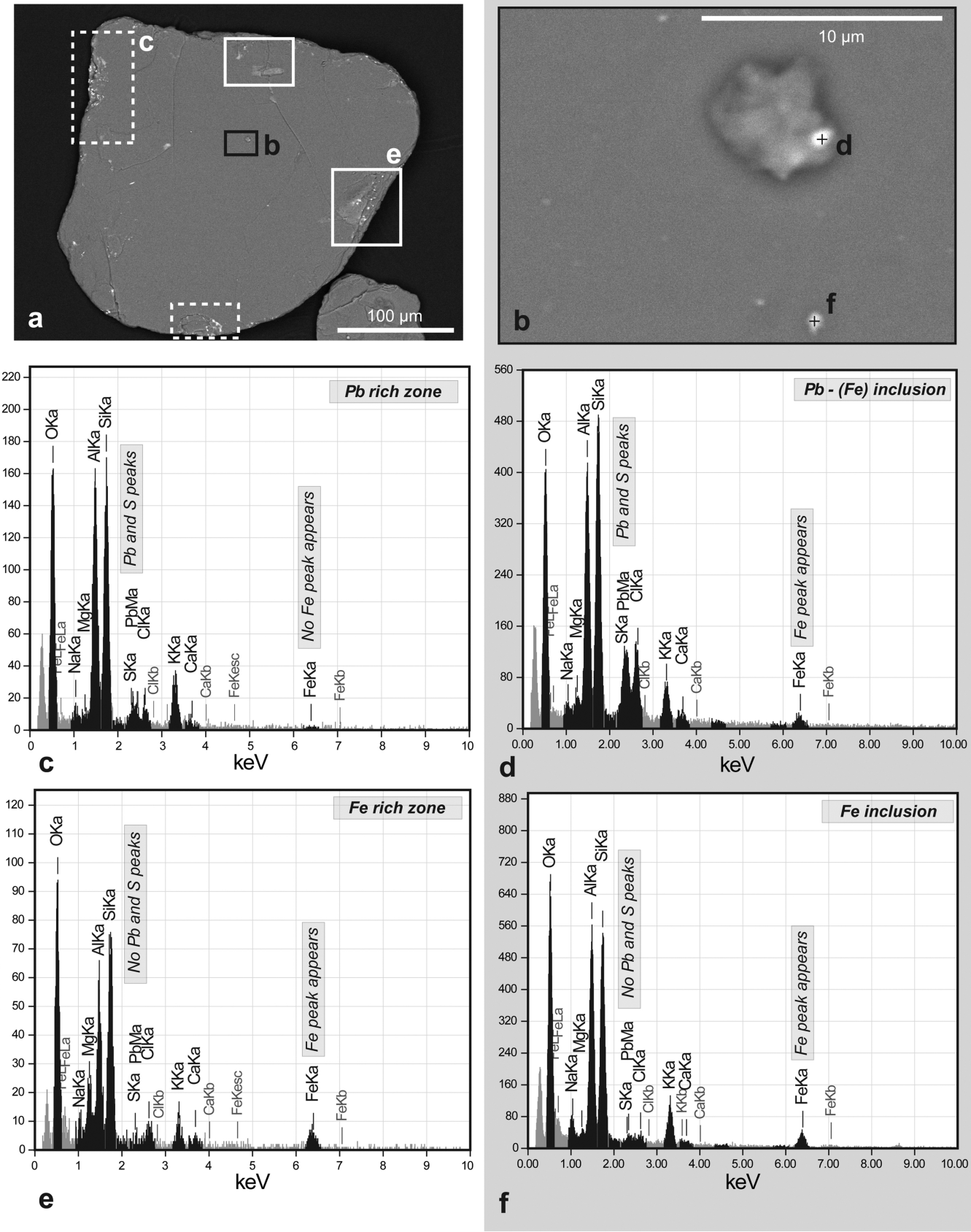
a
c
b
e
100 µm
b
10 µm
d
f
Pb rich zone
Counts
keV
OKa
AlKa
SiKa
Pb and S peaks
No Fe peak appears
MgKa
PbMa
ClKa
NaKa
SKa
KKa
CaKa
ClKb
CaKb
FeKesc
FeKa
FeKb
c
Pb - (Fe) inclusion
Fe peak appears
d
Fe rich zone
No Pb and S peaks
e
Fe inclusion
f

Figure 7

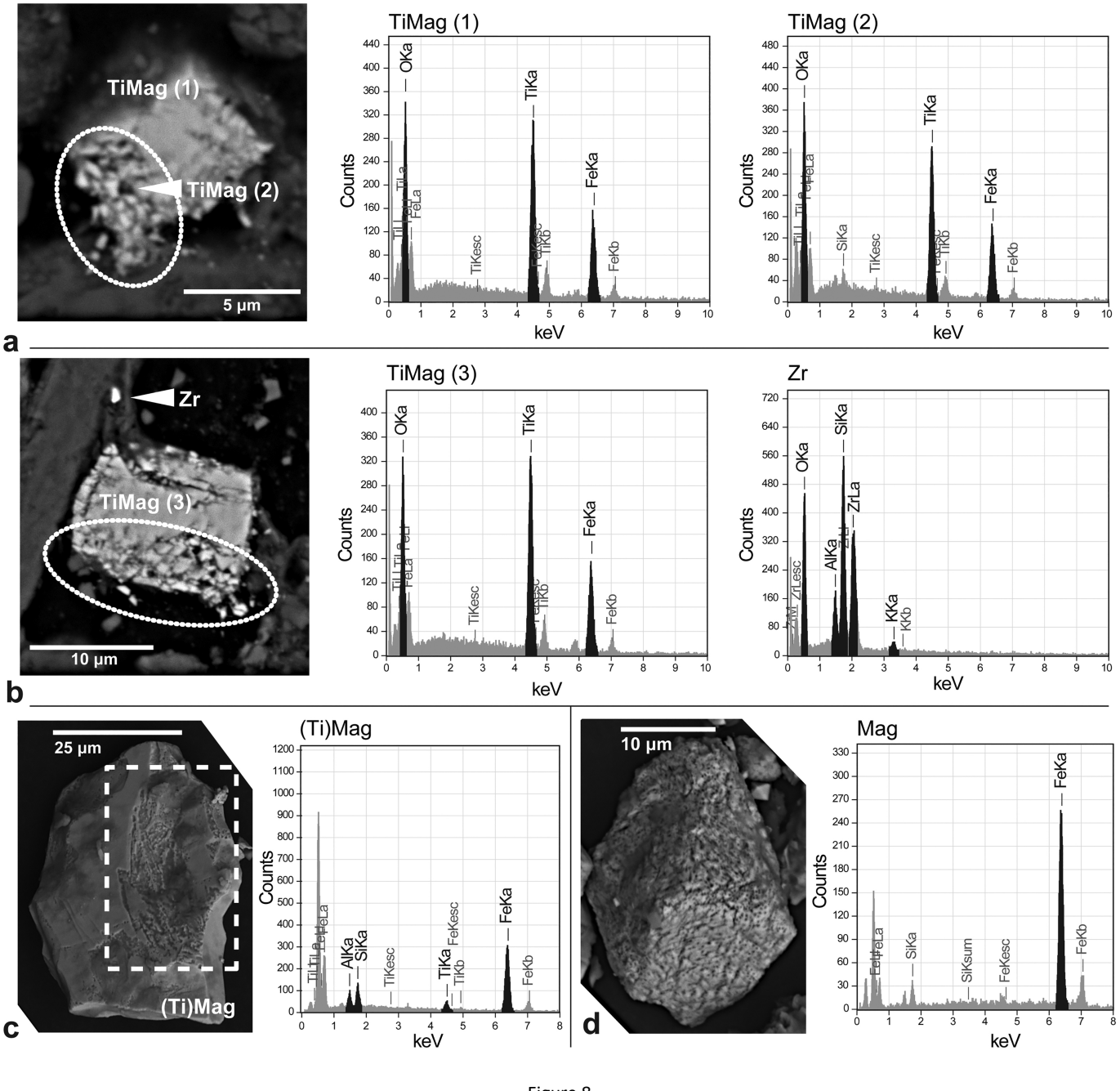
a
TiMag (1)
TiMag (2)
5 µm
TiMag (1)
TiMag (2)
Counts
keV
OKa
TiKa
FeKa
TiKesc
FeKb
SiKa
b
Zr
TiMag (3)
10 µm
TiMag (3)
Zr
OKa
TiKa
FeKa
SiKa
ZrLa
AlKa
KKa
c
25 µm
(Ti)Mag
(Ti)Mag
AlKa
SiKa
TiKa
FeKesc
d
10 µm
Mag
SiKsum

Figure 8

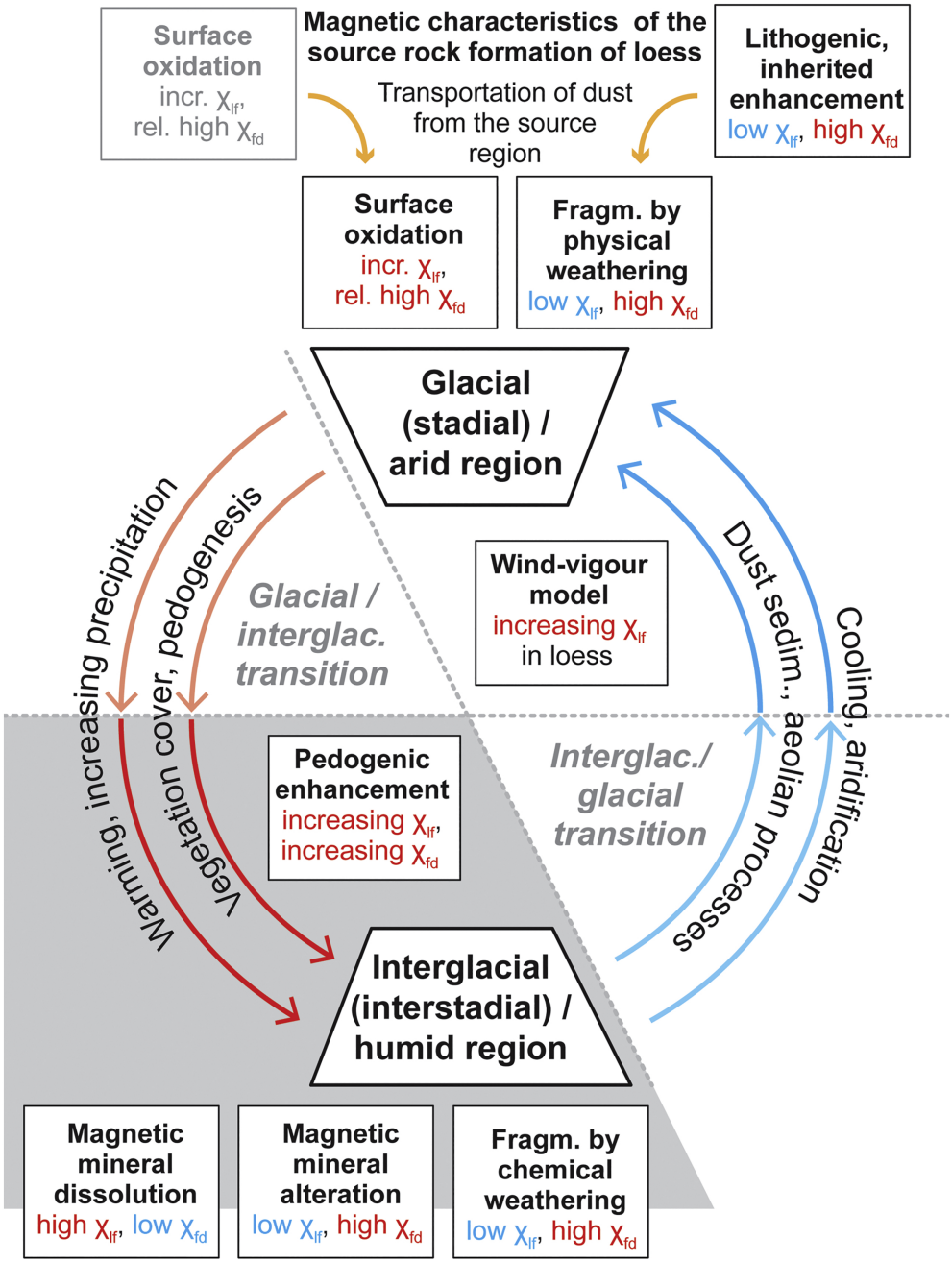
Surface oxidation
incr. χ_{lf},
rel. high χ_{fd}
Magnetic characteristics of the source rock formation of loess
Transportation of dust from the source region
Lithogenic, inherited enhancement
low χ_{lf}, high χ_{fd}
Surface oxidation
incr. χ_{lf},
rel. high χ_{fd}
Fragm. by physical weathering
low χ_{lf}, high χ_{fd}
Glacial (stadial) / arid region
Warming, increasing precipitation
Vegetation cover, pedogenesis
Glacial / interglac. transition
Wind-vigour model
increasing χ_{lf}
in loess
Dust sedim., aeolian processes
Cooling, aridification
Pedogenic enhancement
increasing χ_{lf},
increasing χ_{fd}
Interglac./ glacial transition
Interglacial (interstadial) / humid region
Magnetic mineral dissolution
high χ_{lf}, low χ_{fd}
Magnetic mineral alteration
low χ_{lf}, high χ_{fd}
Fragm. by chemical weathering
low χ_{lf}, high χ_{fd}

Figure 9